UC San Diego
UC San Diego Previously Published Works

Title

mTORC2 controls the activity of PKC and Akt by phosphorylating a conserved TOR interaction motif

Permalink

https://escholarship.org/uc/item/296334vd

Journal

Science Signaling, 14(678)

ISSN

1945-0877

Authors

Baffi, Timothy R
Lordén, Gema
Wozniak, Jacob M
et al.

Publication Date

2021-04-13

DOI

10.1126/scisignal.abe4509

Peer reviewed

mTORC2 controls the activity of PKC and Akt by phosphorylating a conserved TOR interaction motif

Timothy R. Baffi[1,2], Gema Lordén[1], Jacob M. Wozniak[1,2,3], Andreas Feichtner[4], Wayland Yeung[5,6], Alexandr P. Kornev[1], Charles C. King[1], Jason C. Del Rio[1,2], Ameya J. Limaye[7], Julius Bogomolovas[8], Christine M. Gould[1,2], Ju Chen[8], Eileen J. Kennedy[7], Natarajan Kannan[5,6], David J. Gonzalez[1,3], Eduard Stefan[4], Susan S. Taylor[1,9], Alexandra C. Newton[1]*

The complex mTORC2 is accepted to be the kinase that controls the phosphorylation of the hydrophobic motif, a key regulatory switch for AGC kinases, although whether mTOR directly phosphorylates this motif remains controversial. Here, we identified an mTOR-mediated phosphorylation site that we termed the TOR interaction motif (TIM; F-x$_3$-F-pT), which controls the phosphorylation of the hydrophobic motif of PKC and Akt and the activity of these kinases. The TIM is invariant in mTORC2-dependent AGC kinases, is evolutionarily conserved, and co-evolved with mTORC2 components. Mutation of this motif in Akt1 and PKCβII abolished cellular kinase activity by impairing activation loop and hydrophobic motif phosphorylation. mTORC2 directly phosphorylated the PKC TIM in vitro, and this phosphorylation event was detected in mouse brain. Overexpression of PDK1 in mTORC2-deficient cells rescued hydrophobic motif phosphorylation of PKC and Akt by a mechanism dependent on their intrinsic catalytic activity, revealing that mTORC2 facilitates the PDK1 phosphorylation step, which, in turn, enables autophosphorylation. Structural analysis revealed that PKC homodimerization is driven by a TIM-containing helix, and biophysical proximity assays showed that newly synthesized, unphosphorylated PKC dimerizes in cells. Furthermore, disruption of the dimer interface by stapled peptides promoted hydrophobic motif phosphorylation. Our data support a model in which mTORC2 relieves nascent PKC dimerization through TIM phosphorylation, recruiting PDK1 to phosphorylate the activation loop and triggering intramolecular hydrophobic motif autophosphorylation. Identification of TIM phosphorylation and its role in the regulation of PKC provides the basis for AGC kinase regulation by mTORC2.

INTRODUCTION

Activation of nearly all eukaryotic protein kinases involves the structuring of an activation loop segment in the kinase domain, most commonly achieved by phosphorylation (1). The activation loop of AGC kinase family members (2, 3), including protein kinase C (PKC) and Akt, is phosphorylated directly by the phosphoinositide-dependent kinase-1 (PDK1) (4–6). AGC kinases additionally have a C-terminal extension of the kinase domain (C-tail) that harbors a conserved phosphorylation site, the hydrophobic motif (7, 8), which regulates their activity (9, 10). The mechanistic target of rapamycin complex 2 (mTORC2) regulates the phosphorylation of the C-tail sites for a subset of AGC kinases, including most (but not all) PKC isozymes and Akt, by a mechanism that has remained elusive. Given the prevalence of mTOR inhibitor development for various diseases (11), understanding the biochemical mechanisms of how mTORC2 controls AGC kinase function is of critical importance.

For PKC to become catalytically competent, newly synthesized enzyme is matured by constitutive phosphorylation at three conserved

sites (7): the activation loop phosphorylated by PDK1 (6, 12) and two phosphorylation events in the C-tail, the turn motif and hydrophobic motif, which are mTORC2 sensitive for all but three of the nine PKC isozymes (13, 14). The activation loop and hydrophobic motif phosphorylation events are required for cellular PKC activity (10, 15); in contrast, turn motif phosphorylation is not necessary for catalysis and instead promotes protein stability (16). For Akt, turn motif phosphorylation occurs cotranslationally at the ribosome by direct mTORC2 phosphorylation (17). In contrast, phosphorylation of the activation loop and hydrophobic motif sites is agonist-evoked (18), dependent on the generation of phosphatidylinositol (3,4)-bisphosphate or phosphatidylinositol (3,4,5)-trisphosphate (PIP$_3$) at cellular membranes (19–22). The Akt hydrophobic motif phosphorylation, distinct from that of PKC, enhances Akt activity (23) but is not required for catalysis (24); rather, activation loop phosphorylation is necessary and sufficient for Akt activity (25). Thus, hydrophobic motif phosphorylation of PKC is constitutive and controls the steady-state levels of PKC, whereas phosphorylation of the corresponding site in Akt is agonist dependent and controls the acute activity of Akt, but not its stability. Phosphorylation of the hydrophobic motif is opposed by the pleckstrin homology (PH) domain leucine-rich repeat protein phosphatase (PHLPP), with dephosphorylation promoting the down-regulation of PKC and the inactivation of Akt (26). The dysregulation of the hydrophobic motif phosphorylation on both kinases in cancer highlights the importance of understanding the mechanism of phosphorylation.

The current dogma proposes that the atypical kinase complex mTORC2 is the long-sought-after "hydrophobic motif kinase" (27) that directly activates several AGC kinases by phosphorylating the turn motif and hydrophobic motif sites (28, 29). However, cellular

[1]Department of Pharmacology, University of California at San Diego, La Jolla, CA 92093, USA. [2]Biomedical Sciences Graduate Program, University of California at San Diego, La Jolla, CA 92093, USA. [3]Skaggs School of Pharmacy and Pharmaceutical Sciences, University of California at San Diego, La Jolla, CA 92093, USA. [4]Institute of Biochemistry and Center for Molecular Biosciences, University of Innsbruck, Innsbruck A-6020, Austria. [5]Institute of Bioinformatics, University of Georgia, Athens, GA 30602, USA. [6]Department of Biochemistry and Molecular Biology, University of Georgia, Athens, GA 30602, USA. [7]Department of Pharmaceutical and Biomedical Sciences, College of Pharmacy, University of Georgia, Athens, GA 30602, USA. [8]Department of Medicine, University of California at San Diego, La Jolla, CA 92093, USA. [9]Department of Chemistry and Biochemistry, University of California at San Diego, La Jolla, CA 92093, USA.
*Corresponding author. Email: anewton@health.ucsd.edu

and biochemical studies point to autophosphorylation controlling this site. First, the catalytic competence of both PKC and Akt is required for hydrophobic motif phosphorylation in cells (30, 31). Second, autophosphorylation at this site on the purified kinases is triggered in vitro by PDK1 phosphorylation of the activation loop (6, 32). Third, pure PKC selectively dephosphorylated at the hydrophobic motif in vitro reautophosphorylates at this site by an intramolecular mechanism (31). In addition, we have previously reported that hydrophobic motif phosphorylation of Akt, but not that of kinase-inactive Akt, is induced in the absence of mTORC2 by any signal that disengages the PH domain of Akt from its kinase domain, as occurs upon binding to the plasma membrane (33). These results suggest that phosphate incorporation at the hydrophobic motif is governed by a kinase-intrinsic mechanism. The related AGC kinases serum/glucocorticoid-regulated kinase (SGK), protein kinase C–related kinase (PKN), and ribosomal s6 kinase (RSK) also depend on mTORC2, (34–37), which is evolutionarily conserved in yeast (38). In contrast, hydrophobic motif phosphorylation of the AGC kinase member S6K depends on mTORC1 (39–41). Contributing to the puzzle of understanding mTORC2 regulation, three novel PKCs (δ, θ, and η) are mTOR independent and do not require mTOR kinase activity for phosphorylation (13). Thus, in the absence of a mechanism for hydrophobic motif phosphorylation, the function of mTORC2 in regulating AGC kinases remains unclear.

Here, we identified a distinct AGC kinase phosphorylation site regulated by mTORC2, which we termed the TOR interaction motif (TIM) that controls the activation of PKC and Akt by facilitating PDK1 phosphorylation of the activation loop. The phosphorylation of the PKC and Akt hydrophobic motif was governed by autophosphorylation in an mTORC2- and PDK1-dependent manner. We detected phosphorylation of Thr^{634} in the PKCβII TIM by mass spectrometry (MS) in mouse brain and showed that mTORC2 phosphorylated the TIM site in vitro. TIM phosphorylation was sensitive to mTOR inhibition and mTORC2 deficiency in cells, and mutation of the TIM site abolished PKC and Akt cellular kinase activity by impairing activation loop and hydrophobic motif phosphorylation. Accordingly, we showed that TIM phosphorylation in PKC activation resulted in conformational rearrangements that promoted PDK1 docking to the C-tail. Reanalysis of a PKCβII crystal structure reveals a PKC homodimer that is regulated by TIM phosphorylation and mTOR activity. Targeting the TIM dimer interface with stapled peptides was sufficient to enhance PKC phosphorylation in cells. Thus, these data are consistent with a model in which mTORC2 phosphorylates nascent PKC at the TIM and turn motif sites to relieve dimerization and expose the PDK1 binding site in the C-tail, leading to transphosphorylation of the activation loop and intramolecular autophosphorylation at the hydrophobic motif. In addition, we showed that the TIM consensus sequence (F-x$_3$-F-T) is evolutionarily conserved in AGC kinases from major eukaryotic clades and coevolved with TOR complex components, suggesting ancient origins for mTORC2-dependent regulation of AGC kinases.

RESULTS

PKC maturation is defective upon loss of mTORC2

The phosphorylation of most PKC isozymes, including the conventional PKCs (α, β, and γ) and all Akt isozymes (Akt1, Akt2, and Akt3) (Fig. 1A), depends on mTORC2, which ultimately controls the enzymatic activity and cellular stability of these kinases (13, 14). To

assess the nature of the mTORC2 requirement, we characterized PKC function in stress-activated map kinase-interacting protein 1 (Sin1) knockout (KO) ($Sin1^{-/-}$) and rapamycin-insensitive companion of mTOR (Rictor) KO ($Ric^{-/-}$) mouse embryonic fibroblasts (MEFs), which lack critical components of the mTORC2 complex and abolish mTORC2 function (42–45). Endogenous PKC phosphorylation at the activation loop, turn motif, and hydrophobic motif sites was ablated in Sin1 KO and Rictor KO MEFs (Fig. 1B). In addition, the steady-state levels of PKC were reduced, consistent with the unphosphorylated species of PKC being unstable (46). Accompanying the reduced PKC levels, the cellular activity of PKC was reduced in Sin1 KO MEFs compared to wild-type (WT) MEFs as assessed using the C kinase activity reporter (CKAR) (Fig. 1C and fig. S1A) (47, 48). Similarly, mTOR inhibition with the mTORC1/2 inhibitor Torin (49), but not the mTORC1-specific inhibitor rapamycin, also impaired PKC phosphorylation (Fig. 1D), which could not be rescued by agonist stimulation, targeting to the plasma membrane or protecting PKC from dephosphorylation with active-site inhibitors (fig. S1, B to E) (50). Thus, mTOR activity and mTORC2 complex integrity are necessary for PKC function, the loss of which results in an unphosphorylated, inactive, and unstable enzyme.

To further characterize the PKC defect in the absence of mTORC2, we used a live-cell PKC conformation reporter, Kinameleon, which detects intramolecular rearrangements of functional PKC by increases in the Förster resonance energy transfer (FRET) ratio between cyan fluorescent protein (CFP) and yellow fluorescent protein (YFP) flanking the N and C termini of the enzyme (51). The PKCβII-Kinameleon reporter exhibits increasing FRET ratios in each of the conformation transitions: (i) Unprimed (unphosphorylated) has the lowest FRET ratio, (ii) primed (phosphorylated and autoinhibited) has an intermediate FRET ratio, and (iii) active (membrane-associated) has the highest FRET ratio. Consistent with a role for mTORC2 in PKC priming, PKCβII-Kinameleon expressed in Sin1 KO MEFs displayed a reduced FRET ratio compared to that in Sin1 KO MEFs reconstituted with Sin1; this low FRET ratio was similar to that of kinase-dead PKCβII [kdPKC; K371R (52)], which is incapable of priming because it cannot autophosphorylate (Fig. 1E). PKCβII-Kinameleon expressed in Sin1 KO MEFs also did not undergo a FRET change upon activation in response to phorbol 12,13-dibutyrate (PDBu) stimulation; likewise, unprimed kdPKC did not undergo a conformational change because it cannot transition to the primed or active conformations, which are predicated on autophosphorylation (Fig. 1F) (46). However, reconstitution of Sin1 into Sin1 KO MEFs rescued the phenotype and allowed PKC to display a FRET change characteristic of primed PKC activation (Fig. 1F). These data reveal that mTORC2 promotes the mature, autoinhibited conformation of PKC.

As an additional measure of the PKC folding deficiency in the absence of mTORC2, we used an FRET-based translocation assay to assess PKC ligand sensitivity in living cells. We have previously shown that unprimed PKC translocates to plasma membrane more rapidly than primed PKC upon agonist stimulation, owing to exposed ligand-binding C1 domains; these domains become masked in primed (phosphorylated) and autoinhibited PKC. Consistent with the characteristics of unprimed enzyme, WT PKCβII translocated more rapidly from the cytosol to plasma membrane in Sin1 KO MEFs ($Sin1^{-/-}$ + PKC) compared with WT MEFs ($Sin1^{+/+}$ + PKC) (Fig. 1, G and H). Reconstitution of Sin1 KO MEFs with Sin1 ($Sin1^{-/-}$ + PKC + Sin1) slowed the translocation rate to that observed in WT MEFs. The enhanced rate of PKC translocation in mTORC2-deficient
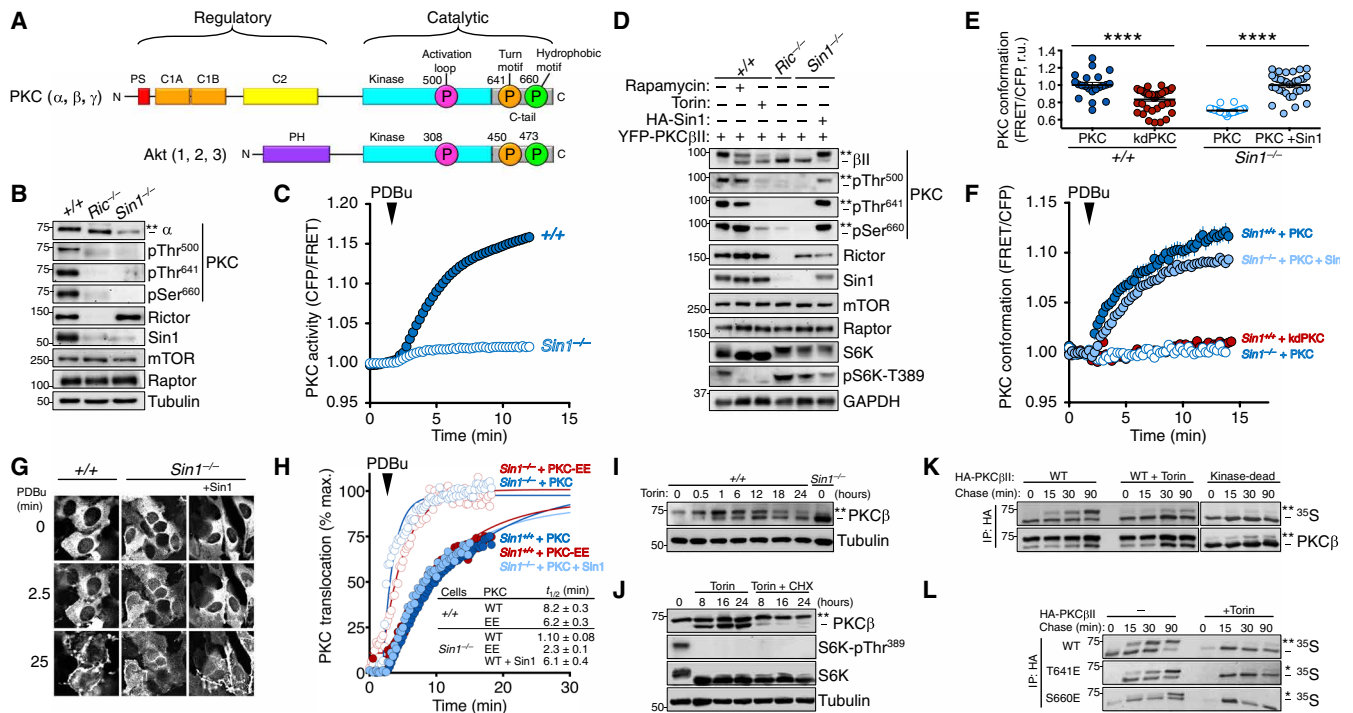
Fig. 1. Defect in PKC maturation upon loss of mTORC2. (**A**) Schematic of conventional PKC (cPKC) and Akt domain structures. cPKCs (α, β, and γ) have an autoinhibitory pseudosubstrate (PS; red), tandem diacylglycerol sensing C1 domains (orange), and a Ca²⁺-dependent plasma membrane sensing C2 domain (yellow) in their N-terminal regulatory moiety and a kinase domain (cyan) and C-terminal tail (C-tail; gray) in the catalytic moiety. Akt has a PIP₃-sensing PH domain (purple) and a kinase domain (cyan) and C-terminal tail (C-tail; gray) in the catalytic moiety. Both kinases have three conserved phosphorylation sites at the activation loop (magenta) of the kinase domain and the turn motif (orange) and hydrophobic motif (green) in the C-tail, indicated with circles (PKCβII and Akt1 numbering). For PKC, these phosphorylation events are constitutive, whereas for Akt, only the phosphorylation event in the turn motif is constitutive, with the activation loop and hydrophobic motif phosphorylated in an agonist-dependent manner. (**B**) Western blot of Triton-solubilized lysates from WT (+/+), Rictor KO (*Ric⁻/⁻*), or Sin1 KO (*Sin1⁻/⁻*) MEFs probed with the indicated total and phospho-specific antibodies. The double asterisks (**) denote the position of mature, fully phosphorylated PKC, and the dash (–) indicates the position of unphosphorylated PKC. Note that phosphorylation of the activation loop does not cause a mobility shift and this site is modified in C-terminally phosphorylated species. Blots are representative of three independent experiments. (**C**) PKC activity in WT (+/+) or Sin1 KO (*Sin1⁻/⁻*) cells expressing the PKC activity reporter CKAR and treated with PDBu (200 nM) to maximally activate PKC. Data represent the normalized FRET ratio changes (means ± SEM) from three independent experiments. (**D**) Western blot of Triton-solubilized lysates from WT (+/+), Rictor KO (*Ric⁻/⁻*), or Sin1 KO (*Sin1⁻/⁻*) MEFs, expressing YFP-PKCβII and HA-Sin1, treated with rapamycin (10 nM; 24 hours) or Torin (200 nM; 24 hours), and probed with the indicated antibodies. Mobility shifts were as described in (B). Blots are representative of three independent experiments. GAPDH, glyceraldehyde-3-phosphate dehydrogenase. (**E**) Basal conformation of PKC analyzed using the conformational reporter Kinameleon that comprises a donor:acceptor pair flanking the N and C termini of PKC. Autoinhibited PKC has a low FRET ratio, and the open conformation has a high FRET ratio. Indicated are the FRET ratio (means ± SEM) of PKCβII Kinameleon wild-type (WT) or kinase-dead K371R (kd) expressed without or with HA-Sin1 in WT (+/+) or Sin1 KO (*Sin1⁻/⁻*) MEFs. Each data point represents the FRET ratio from an individual cell relative to the average maximum signal in three independent experiments. r.u., relative units. ****$P < 0.0001$ by Student's t test. (**F**) Agonist-induced conformational changes of PKCβII assessed using the reporter Kinameleon. WT or kinase-dead K371R (kd) Kinameleon was expressed without or with HA-Sin1 in WT (*Sin1⁺/⁺*) or Sin1 KO (*Sin1⁻/⁻*) MEFs and treated with PDBu (200 nM) at the indicated time. Data represent the normalized FRET ratio changes (means ± SEM) from three independent experiments. (**G**) Fluorescence images of WT (+/+) or Sin1 KO (*Sin1⁻/⁻*) MEFs expressing PKCβII Kinameleon alone or with coexpression of HA-Sin1, before (0) or after treatment with PDBu (200 nM) for the indicated times. Images are representative of three independent experiments. (**H**) Analysis of plasma membrane translocation of mYFP-PKCβII WT or T641E/S660E (EE) in WT (+/+) or Sin1 KO (–/–) MEFs coexpressing myristoylated-palmitoylated mCFP with or without HA-Sin1 and treated with PDBu (100 nM). Data represent the FRET ratio signal from the CFP to YFP and are normalized to the maximum FRET ratio signal determined by fitting the data to a single-phase logarithmic nonlinear regression (solid lines). Data represent the normalized FRET ratio changes (means ± SEM) from three independent experiments. (**I**) Western blot of Triton-solubilized lysates from WT (+/+) MEFs overexpressing PKCβII and treated with Torin (250 nM) for 24 hours before lysis. Mobility shifts were as described in (B). Blots are representative of three independent experiments. (**J**) Western blot of Triton-solubilized lysates from COS7 cells transfected with cDNA for PKCβII for 24 hours before treatment with Torin (250 nM) and CHX (250 μM) for the indicated times. Mobility shifts were as described in (B). Blots are representative of three independent experiments. (**K**) Autoradiogram (detecting ³⁵S-labeled newly synthesized PKC) and Western blot (detecting total pool of PKC) of HA immunoprecipitates (IP) from a pulse-chase analysis of COS7 cells expressing HA-PKCβII WT or K371R (kinase-dead) and treated with Torin (250 nM) during the chase. Mobility shifts were as described in (B). Blots are representative of three independent experiments. (**L**) Autoradiogram (detecting ³⁵S-labeled newly synthesized PKC) and Western blot (detecting total pool of PKC) HA immunoprecipitates from a pulse-chase analysis of WT MEFs expressing the indicated HA-PKCβII constructs and treated with Torin (250 nM) during the chase. The double asterisks (**) denote the position of mature, fully phosphorylated PKC; the single asterisk (*) denotes the position of PKC phosphorylated at either the turn motif or hydrophobic motif; and the dash (–) indicates the position of unphosphorylated PKC. Blots are representative of three independent experiments.

cells was due to an exposed C1A domain, because impairing ligand binding of the domain by introducing a W58A mutation (*53*) reduced the rate of PKCβII translocation in Rictor KO MEFs

(*Ric⁻/⁻* + PKC-W58A) (fig. S1F). Furthermore, PKC with phosphomimetic Glu substitutions at the turn and hydrophobic motif phosphoacceptor sites (T641E/S660E) translocated rapidly in Sin1 KO MEFs

(Sin1^{−/−} + PKC-EE), indicative of the unprimed conformation of PKC. This finding suggests that mTORC2 regulates PKC conformation by a mechanism independent of phosphorylation at the C-tail turn motif and hydrophobic motif sites (Fig. 1H). This rapid translocation was not a result of the phosphomimetic mutations not allowing the primed, autoinhibited conformation because this same construct translocated slowly in WT MEFs, indicating normal autoinhibition. Thus, mTORC2 promotes the autoinhibited and "primed" conformation of PKC by a mechanism that is independent of phosphorylation of the known C-tail sites.

We next addressed whether mTOR activity regulates the initial phosphorylation of newly synthesized PKC or the steady-state phosphorylation of mature PKC. The stoichiometry of PKC phosphorylation can be assessed by monitoring the electrophoretic mobility shift that accompanies phosphorylation of the two C-terminal sites (7): The slower mobility species (asterisk, upper band) is phosphorylated at both the turn motif and hydrophobic motif sites and the faster mobility species (dash, lower band) is unphosphorylated. Using electrophoretic mobility to assess the phosphorylation state of PKC, we observed that Torin treatment of WT MEFs overexpressing PKCβII resulted in a relatively slow accumulation of unphosphorylated PKCβII (faster electrophoretic mobility). This slow rate of appearance of unphosphorylated PKC contrasted with the rapid loss of phosphate on the mTORC1-regulated S6K1 (Fig. 1I and fig. S1G). Treatment with the protein synthesis inhibitor cycloheximide (CHX) prevented the Torin-dependent accumulation of unphosphorylated PKC without affecting the amount of preexisting phosphorylated PKC, revealing that mTORC2 exclusively controlled the ability of newly synthesized PKC to become phosphorylated (Fig. 1J). Thus, mTORC2 controls the initial phosphorylation in the maturation of PKC and does not affect the phosphorylation of primed PKC.

To examine the mechanism by which mTORC2 controls the maturation of PKC, we took advantage of pulse-chase experiments to interrogate the pool of newly synthesized enzyme. Cells were metabolically labeled with ^{35}S-Cys/Met for 7 min and then chased with unlabeled amino acids for up to 90 min. PKC was immunoprecipitated and the phosphorylation state of newly synthesized PKC monitored by the electrophoretic mobility shift accompanying C-tail phosphorylation events. As reported previously, PKC matured with a half-time of about 30 min (Fig. 1K) (54). The presence of the mTOR inhibitor during the chase prevented PKC progression to the slower-mobility phosphorylated species, similar to the inability of a kinase-deficient PKC mutant to progress to the phosphorylated species (Fig. 1K). Phosphomimetic Glu substitutions at the turn (T641E) or hydrophobic (S660E) motifs did not rescue PKC phosphorylation upon mTOR inhibition, revealing that neither site can bypass the rate-limiting mTORC2 requirement in PKC processing (Fig. 1L and fig. S1H). Together, mTORC2 regulates PKC activity, conformation, and the rate-limiting step of PKC phosphorylation independently of the turn motif and hydrophobic motif sites.

The hydrophobic motif of PKC and Akt is regulated by autophosphorylation

Given that mTORC2 is the proposed hydrophobic motif kinase (55, 56) but regulates PKC independently of this site, we investigated the mechanism by which mTORC2 regulates the hydrophobic motif phosphorylation. Accordingly, we examined whether mTORC2 facilitates the PDK1-catalyzed phosphorylation of the activation loop, which is necessary for subsequent phosphorylation at the hydrophobic

motif (6, 12). Pulse-chase analyses in the presence of mTOR inhibitors revealed that coexpression of WT PDK1, but not kinase-dead PDK1 (kdPDK1; K110N), rescued the phosphorylation of newly synthesized PKC as assessed by electrophoretic mobility shift (Fig. 2A). Further analysis with phospho-specific antibodies indicated that PDK1 expression restored phosphorylation at the activation loop and hydrophobic motif, but not at the turn motif, both in WT MEFs treated with Torin and in Sin1 KO MEFs (Fig. 2B). Consistent with previous reports that phosphorylation of the PKC hydrophobic motif is governed by autophosphorylation, PDK1 did not rescue hydrophobic motif phosphorylation of kdPKC (K371R) in either Torin-treated WT MEFs or Sin1 KO MEFs (Fig. 2B). Similar rescue of hydrophobic motif phosphorylation by PDK1 overexpression was also observed in Torin-treated COS7 cells and Rictor KO MEFs (fig. S9, A and B). Correlating with the rescue of hydrophobic motif phosphorylation, overexpression of WT PDK1, but not the kinase-dead mutant, restored cellular PKC activity in Torin-treated WT MEFs or Sin1 KO MEFs (Fig. 2C). These results reveal that PDK1 can bypass the requirement for mTORC2 by a mechanism that depends on the intrinsic catalytic activity of both PDK1 and PKC.

Given that Akt is also regulated by PDK1 and mTORC2 (5, 27), we addressed whether the Akt hydrophobic motif in cells lacking mTORC2 could also be rescued by PDK1 by a mechanisms depending on Akt autophosphorylation. The isolated catalytic domain of Akt1 expressed in Sin1 KO cells was not appreciably phosphorylated at the activation loop (Thr[308]), turn motif (Thr[450]), or hydrophobic motif (Ser[473]), as reported previously (33). Similar to our result above with PKC, coexpression of PDK1 rescued Akt phosphorylation at the activation loop and hydrophobic motif sites, but not at the turn motif (Fig. 2D). This restoration of Akt hydrophobic motif phosphorylation required the catalytic activity of both PDK1 and Akt, because kdPDK1 (K110N) or kinase-dead Akt1 (kdAkt; K179M) were ineffective in promoting hydrophobic motif phosphorylation in the absence of mTORC2 (Fig. 2D). kdAkt becomes phosphorylated at the turn motif in an mTORC2-dependent manner (14). Thus, mTORC2 is necessary only for the phosphorylation of the turn motif in both PKC and Akt. PDK1 can effectively restore hydrophobic motif phosphorylation in cells lacking mTORC2 by a mechanism that depends on the intrinsic catalytic activity of both PDK1 and the recipient kinase (Fig. 2E). Together, these data establish that the hydrophobic motif is not a direct mTORC2 target but rather is modified by autophosphorylation after PDK1 phosphorylation of the activation loop. It is the latter event that is controlled by mTORC2. Therefore, for both PKC and Akt, mTORC2 facilitates, but is not required for, phosphorylation events that control the activity of each kinase.

mTORC2 binds to and phosphorylates a conserved TIM

Having established that mTOR is not the physiological hydrophobic motif kinase, we explored the mechanism by which mTORC2 facilitates hydrophobic motif phosphorylation and kinase activation. To identify critical regions for mTOR-mediated PKC and Akt phosphorylation, we pursued a structural approach to mapping the mTORC2 binding site on PKC. Using pulse-chase analysis to label newly synthesized PKC, we found that mTOR and Sin1 coimmunoprecipitated exclusively with the unphosphorylated, newly synthesized PKC (Fig. 3A and fig. S2A). This association with newly synthesized PKC was mediated by determinants primarily in the catalytic domain (fig. S2B). To identify the interaction regions, we performed a peptide array of the PKCβII catalytic domain sequence and asked which
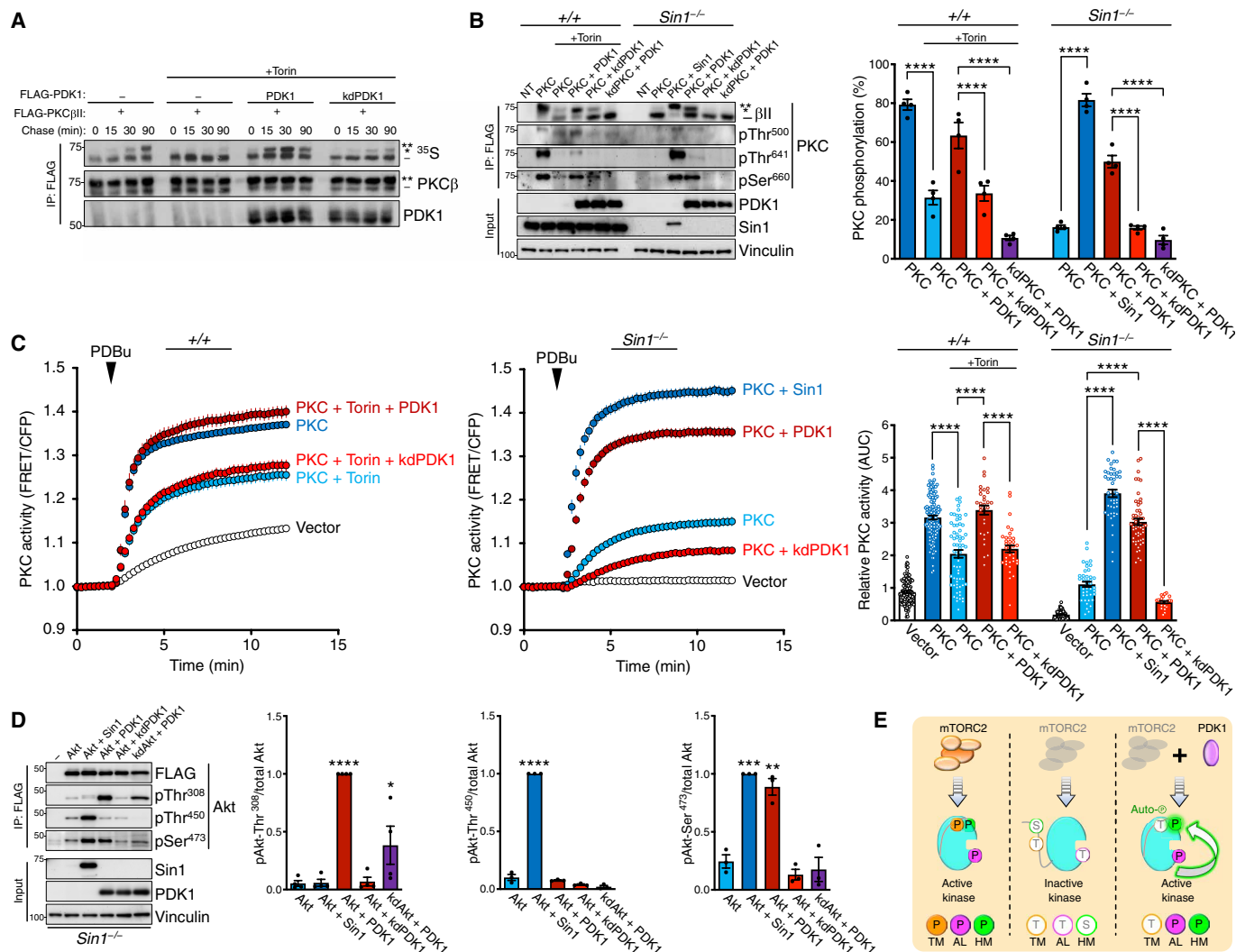
Fig. 2. The hydrophobic motif of PKC and Akt is regulated by autophosphorylation. (**A**) Pulse-chase experiment monitoring newly synthesized FLAG-PKCβII (^{35}S; autoradiograph) immunoprecipitated (IP) from COS7 cells coexpressing FLAG-PDK1 WT or kinase-dead K110N (kdPDK1) and treated without or with Torin (250 nM) during the chase. Blots are representative of three independent experiments. (**B**) Western blot analysis of Triton-solubilized lysates (input) or FLAG immunoprecipitates (IP:FLAG) from WT (+/+) or Sin1 KO ($Sin1^{-/-}$) MEFs expressing FLAG-PKCβII WT or kinase-dead K371R (kdPKC) and FLAG-PDK1 WT, kinase-dead K110N (kdPDK1), or HA-Sin1. Nontransfected cells (NT) also shown. Cells were treated with or without Torin (200 nM) during transfection and lysed 24 hours later. Right: Quantification of the percentage of PKC phosphorylation obtained from the ratio of the slower mobility species (phosphorylated on hydrophobic motif, indicated by asterisks) over total PKC from four independent experiments. (**C**) PKC activity in WT (+/+) or Sin1 KO ($Sin1^{-/-}$) MEFs expressing CKAR2 (48) and mCherry-PKCβII and treated with PDBu (200 nM). Data represent the normalized FRET ratio changes (means ± SEM) from three independent experiments. Right: Quantification of PKC activity reflects the normalized AUC from baseline of 1.0 (means ± SEM) 10 min after PDBu treatment. Each point represents data from one cell. (**D**) Western blot analysis of Triton-solubilized lysates (input) or FLAG immunoprecipitates (IP:FLAG) from Sin1 KO ($Sin1^{-/-}$) MEFs expressing FLAG-mAkt1 catalytic domain (141 to 480) WT or kinase-dead K179M (kd) and FLAG-PDK1 WT, kinase-dead K110N (kd), or HA-Sin1. Right: Quantification of Akt phosphorylation reflects the normalized phospho-signal relative to total Akt for the activation loop (pThr308), turn motif (pThr450), or hydrophobic motif (pSer473) from four independent experiments. (**E**) The hydrophobic motif of PKC and Akt is regulated by autophosphorylation in a PDK1-dependent and mTORC2-sensitive manner. Schematic of mTORC2 and PDK1 function in the phosphorylation of PKC and Akt. Left: mTORC2-containing cells produce kinase that is phosphorylated at the activation loop (AL), turn motif (TM), and hydrophobic motif (HM). Middle: mTORC2-deficient cells produce kinase with impaired phosphorylation at all three sites. Right: PDK1 overexpression in mTORC2-deficient cells rescues phosphorylation at the AL and HM, but not at the TM. This rescue depends on the intrinsic catalytic activity of PKC and Akt, indicating that the hydrophobic motif of both kinases is regulated by autophosphorylation (green arrow) in a reaction that is promoted by PDK1-mediated phosphorylation of the activation loop. mTORC2 facilitates the PDK1 step and can by bypassed with PDK1 overexpression. In Western blots, the double asterisks (**) denote the position of mature, phosphorylated PKC; the single asterisk (*) denotes the position of PKC phosphorylated at the hydrophobic motif; and the dash (–) indicates the position of unphosphorylated PKC. *$P < 0.05$, **$P < 0.01$, ***$P < 0.001$, and ****$P < 0.0001$ by one-way ANOVA and Tukey post hoc test. Western blot quantifications represent the means ± SEM from at least three independent experiments.

segments bound mTORC2 components. Specifically, 15-mer synthesized peptides derived from the kinase + C-tail (amino acids 296 to 673), at one residue intervals, were spotted onto a membrane that

was overlaid with lysate from cells expressing Sin1, regulatory-associated protein of mTOR (Raptor), or mTOR. Both components of mTORC2 (mTOR and Sin1), but not the mTORC1 subunit Raptor, bound
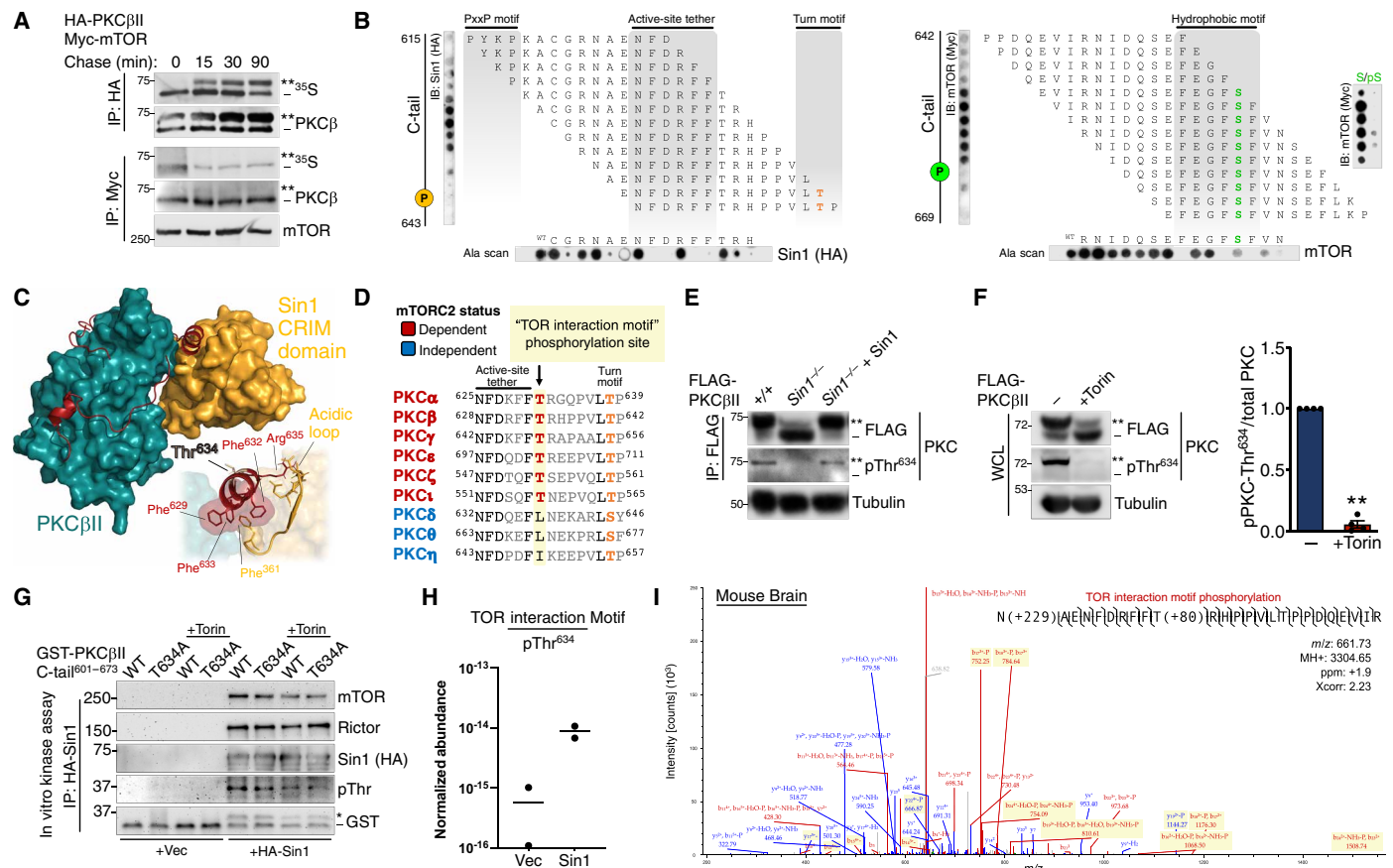
Fig. 3. mTORC2 binds to and phosphorylates a TIM. (**A**) Autoradiograph (^{35}S) and Western blot of HA or Myc immunoprecipitates from a pulse-chase experiment of COS7 cells coexpressing HA-PKCβII and Myc-mTOR. The double asterisks (**) denote the position of mature, fully phosphorylated PKC, and the dash (–) indicates the position of unphosphorylated PKC. Blots are representative of three independent experiments. (**B**) Top: Immunoblot (IB) analysis of one-step, 15-mer peptide arrays spanning residues 615 to 643 (left) and residues 642 to 669 (right) of the PKCβII C-tail overlaid with Triton-solubilized lysate from WT MEFs expressing HA-Sin1 or Myc-mTOR and probed with antibodies for Sin1 (HA) or mTOR (Myc). The positions of the turn motif Thr^{641} and hydrophobic motif Ser^{660} are indicated. Far right: Peptide arrays of the indicated hydrophobic motif sequences were generated with phospho-Ser (pS) or unphosphorylated Ser (S) at the hydrophobic motif site and probed for mTOR as in panels on left. Bottom: Ala scans of the indicated C-tail peptides were probed for Sin1 (HA) and mTOR; first spot is the WT peptide. Blots are representative of three independent experiments. (**C**) Docking of the Sin1 CRIM domain (nuclear magnetic resonance structure, PDB ID: 2RVK) to the PKCβII catalytic domain (x-ray structure, PDB ID: 2I0E). Inset: Interactions of the CRIM domain acidic loop with the PKCβII TIM helix are shown. (**D**) Sequence alignment of the active-site tether and turn motif regions in the PKC C-tail, indicating the TIM-Thr conserved in mTORC2-dependent PKC isozymes. (**E**) Western blot of FLAG immunoprecipitates (IP: FLAG) from WT (+/+) or Sin1 KO (Sin1$^{-/-}$) MEFs expressing FLAG-PKCβII alone or with HA-Sin1 and probed with an antibody to pThr^{634} or FLAG. Tubulin blot represents 10% whole-cell lysate input before immunoprecipitation. Blots are representative of three independent experiments. (**F**) Western blot of whole-cell lysate (WCL) from HEK293T cells expressing FLAG-PKCβII, treated with Torin (250 nM) for 36-hour cotransfection, and probed with the indicated antibodies. Right: Quantification reflects the TIM phospho-signal (pThr^{634}) relative to total PKC. (**G**) Western blot from in vitro mTORC2 kinase assay, performed by incubation of HA-Sin1 or HA empty vector control (Vec) immunoprecipitated from HEK293T cells transfected with these HA constructs, and GST-tagged PKCβII C-tail (amino acid residues 601 to 673) WT or T634A purified by GST pull-down, in the presence or absence of Torin (200 nM) and probed with the indicated antibodies. The single asterisk (*) indicates phosphorylated GST-PKCβII C-tail peptide, and the dash (–) indicates unphosphorylated peptide. (**H**) Relative abundance of PKCβII C-tail peptide or phosphorylation at Thr^{634} for the in vitro kinase assay shown in (H) as determined by LC-MS. Data were obtained from two independent kinase assays. (**I**) Representative spectrum of in vivo PKCβII Thr^{634} phosphorylation from analysis of a mouse brain phospho-proteomic dataset. Blue color denotes y ions, and red color denotes b ions. ppm, parts per million; Xcorr, spectral match correlation score; m/z, mass/charge ratio. **$P < 0.01$ by one-way ANOVA and Tukey post hoc test or Student's t test. Error bars represent SEM from at least three independent experiments.

to peptides containing the active-site tether (57) and hydrophobic motif regions in the C-tail (Fig. 3B and fig. S2C). Alanine scanning of the peptide displaying the greatest binding to Sin1 or mTOR identified Phe residues in the PKC active-site tether (PKCβII Phe^{629}, Phe^{632}, and Phe^{633}) and hydrophobic motif (PKCβII Phe^{656}, Phe^{659}, and Phe^{661}) as critical for binding to Sin1 and mTOR, respectively (Fig. 3B). Furthermore, substitution of the hydrophobic motif phospho-acceptor Ser^{660} with phospho-Ser (pS) abolished mTOR binding (Fig. 3B), consistent with mTORC2 specifically associating with

unphosphorylated PKC. To gain insight into the structural determinants mediating this interaction, we modeled the mTORC2:PKC complex by docking the kinase domain of PKCβII (58) with the conserved region in the middle (CRIM) domain of Sin1 (59), which recruits AGC kinases to mTORC2 (60). Corroborating our peptide arrays, unbiased docking positioned the CRIM domain in contact with the PKC active-site tether (Fig. 3C and fig. S4). An acidic loop region of the Sin1 CRIM domain is required for mTORC2-mediated phosphorylation of PKC and Akt (60). Consistent with this finding, our model

revealed that the acidic loop was anchored to the C-tail by hydrophobic interactions between Phe residues in the active-site tether determined in our peptide arrays to be critical for Sin1 binding (Fig. 3C).

To gain insight into how the binding of mTORC2 could affect phosphorylation of the C-terminal sites, we took advantage of the fact that the novel isoform PKCδ is not regulated by mTORC2 yet also has a turn motif and hydrophobic motif that are phosphorylated during maturation. We engineered PKCδ/β chimeras containing the mTORC2-insensitive PKCδ kinase domain fused to PKCβII C-tail fragments (fig. S3A). Substitution of the PKCδ C terminus with 45 amino acids of PKCβII sequence containing the turn motif and hydrophobic motif phosphorylation sites (PKCδ/β TM; PKCδ$^{1-631}$/βII$^{628-673}$) produced a kinase that required mTORC2 for phosphorylation of the turn motif, but not that of the hydrophobic motif in cells (fig. S3B). However, extending the junction eight residues further to include the PKCβII active-site tether (PKCδ/β AST; PKCδ$^{1-622}$/βII$^{620-673}$) resulted in a chimera that was dependent on mTORC2 for turn motif and hydrophobic motif phosphorylation (fig. S3B). Thus, turn motif phosphorylation is controlled by the specific sequences of the mTORC2-dependent and -independent PKCs, respectively, whereas phosphorylation of the hydrophobic motif is regulated by the region preceding the turn motif in the active-site tether. Comparative structural analysis of several AGC kinase C-tails revealed that the critical active-site tether region that confers mTORC2 independence diverges in PKCβII to form the "novel α helix" (fig. S3, C and D) (58), which may provide a structural basis for the differential regulation of PKCs by mTORC2. Therefore, the active-site tether functions as a molecular switch to confer mTORC2-dependent hydrophobic motif phosphorylation, independently of turn motif phosphorylation.

We next hypothesized that a distinct C-tail phosphorylation site in the active-site tether region may account for the requirement of mTORC2 activity in the regulation of a subset of PKCs. Sequence alignment of the PKC active-site tether revealed a Thr preceding the turn motif site (TM-7; Thr^{634} in PKCβII), which we have termed the TIM that is conserved and present only in mTORC2-sensitive PKCs (Fig. 3D). Cellular phosphorylation of the TIM was effectively suppressed in Sin1 KO MEFs (Fig. 3E) or upon mTOR kinase inhibition with Torin (Fig. 3F), as detected by a pThr^{634} antiserum that labeled a species with the same electrophoretic mobility as mature PKC (61). Incubation of PKCβII C-tail peptide (amino acids 601 to 673) with immunoprecipitated mTORC2 (fig. S5A) resulted in phosphorylation of the TIM site in vitro (Fig. 3, G and H). Furthermore, phosphorylation of this site in mouse brain tissue was detected by tandem MS (Fig. 3I and fig. S5B), validating its presence in vivo. Thus, the TIM is a direct mTORC2 phosphorylation site that specifies the mTORC2 dependence of PKC isozymes.

The TIM is evolutionarily conserved in eukaryotes
Next, we investigated the conservation of the TIM phosphorylation site in other AGC kinases. Human kinome analysis revealed that the TIM-Thr, located in an invariant F-x$_3$-F-T motif, was conserved in all known mTORC2-regulated kinases (Fig. 4A). The TIM was also found in the mTORC1-regulated p70S6K family, as well as in p90RSK and mitogen and stress activated protein kinase (MSK) family kinases, which are not known to be regulated by mTOR (Fig. 4, A and B). We note that although conservation of the TIM-Thr does not explicitly signify a phosphorylation site, TIM phosphorylation is detected in several unbiased proteomics studies (62), although to a lesser degree than either the turn motif or hydrophobic motif sites (fig. S6A).

To assess the evolutionary association of the TIM and the presence of TORC2 components, we analyzed diverse species for the presence of kinases harboring the TIM and for the TORC2 components Rictor and Sin1 (Fig. 4C). The majority of species having kinases with the TIM (52 of 55) also contained TORC2 components (Fig. 4C and fig. S7), supporting the role of the TIM as a TORC2-regulated phosphorylation site throughout evolution. Comparative sequence analyses show that the AGC C-terminal tail is well conserved across eukaryotes and the TIM-Thr consistently appeared in major eukaryotic clades within the F-x$_3$-F-T motif of the active-site tether (Fig. 4D and fig. S6A). Patterns of conservation and variation in the C-terminal motifs reveal that constraints on the TIM-Thr were lost within some families and species. For example, the nuclear dbf2-related (NDR) kinase family, which is present in most eukaryotes, consistently lacks the TIM-Thr. Likewise, SGK family members in multicellular eukaryotes (opisthokonta and viridiplantae) have the TIM-Thr, whereas SGKs in unicellular eukaryotes [stramenophiles, alveolates, Rhizaria (SAR); amoebozoa; and excavata] lack the TIM-Thr. (Fig. 4D and fig. S6B). Conserved within all five major eukaryotic clades, the TIM was likely present in the last eukaryotic common ancestor (LECA). An evolutionary study characterizing the widespread conservation of TOR signaling components in eukaryotes suggests that TOR signaling was also conserved in the LECA and has remained vital in almost all eukaryotes (63). Although phylogenetic studies have traced the appearance of the TOR signaling pathways to the earliest eukaryotes, TORC2 is not found in plants. Our data indicate a plant-specific variation in the TIM in which the Phe preceding the TIM-Thr is replaced by a Trp (Fig. 4D and fig. S6, A and B). Thus, the F-x$_3$-W-T motif in plants may reflect a unique variation on TOR signaling compared to eukaryotes that have retained the canonical F-x$_3$-F-T motif. Together, these observations suggest that the TIM is evolutionarily conserved in eukaryotes and may have coevolved with mTORC2 to regulate a subset of AGC kinases.

TIM phosphorylation is critical for PKC and Akt activity
Next, we assessed the effect of TIM phosphorylation on PKC and Akt activity in cells using biosensors for each kinase (48, 64). Although mutation of the TIM (T634A) or turn motif (T641A) alone had minimal effect on PKC activity stimulated by either the natural agonist uridine 5′-triphosphate (UTP) (to transiently elevate diacylglycerol and Ca^{2+}) or PDBu (for long-term activation), mutation at both sites (AA; T634A/T641A) abolished PKC cellular activity (Fig. 5A). In contrast, Akt1 TIM mutation (T443A) alone abolished the constitutive activity of the isolated catalytic domain. Whereas the Akt inhibitor GDC-0068 caused a drop in FRET ratio in cells expressing the WT Akt1 catalytic domain, reflecting the high constitutive activity of the WT kinase domain, this drop was abrogated with the T443A mutation (Fig. 5B). In contrast, mutation of the turn motif (T450A) did not affect the inhibitor-sensitive activity of Akt1 (Fig. 5B). Western blot analysis revealed that mutation of both the TIM and turn motif in PKC and only the TIM in Akt resulted in reduced activation loop and hydrophobic motif phosphorylation of the inactive PKC and Akt TIM mutants (Fig. 5, C and D). The related AGC kinase PKN2, in contrast, showed a greater dependence on the turn motif than the TIM for activation loop phosphorylation, and TIM mutation in PKN1 enhanced activation loop phosphorylation (fig. S8).

Supporting a role for mTORC2 in promoting PKC activation loop phosphorylation, PDK1 bound to the nascent, unphosphorylated PKC species twofold better than to the phosphorylated form, a
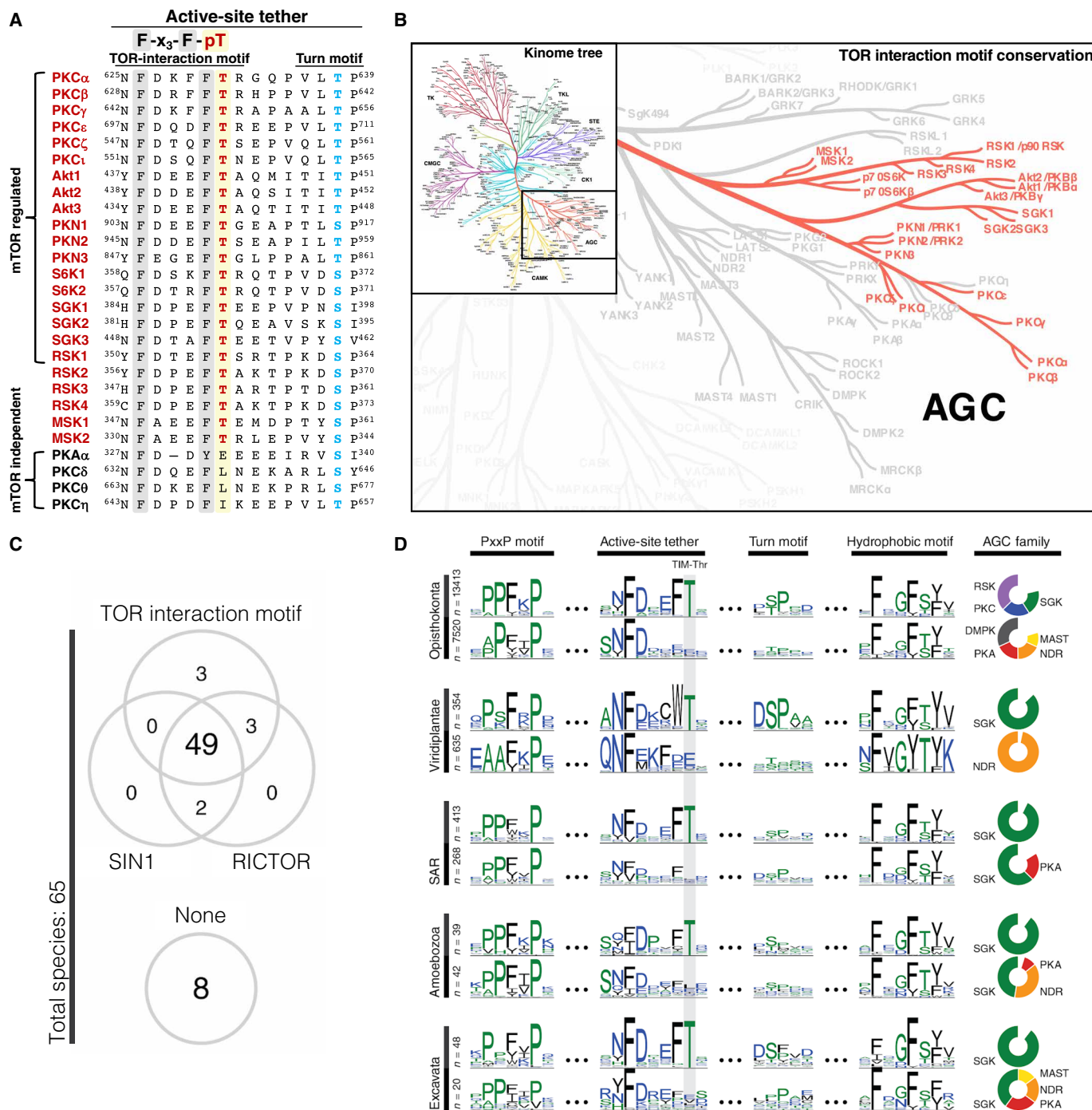
Fig. 4. The TIM is evolutionarily conserved in eukaryotes. (**A**) Sequence alignment of the active-site tether region of AGC kinases indicating the TIM (red) and turn motif (blue) phosphorylation sites for selected AGC kinases. (**B**) AGC kinase branch of the human kinome tree (*110*) indicating conservation of the TIM-Thr in the highlighted kinases. (**C**) Coconservation of the TIM with TORC2 components SIN1 and RICTOR in various species (detailed in fig. S7). Conservation of the TIM was defined by species that showed at least one AGC kinase conserving the TIM-Thr. (**D**) Conservation of the TIM-Thr in the AGC C-terminal tail across five major taxonomic groups. Sequence logos are shown for four distinct regions of the AGC tail: PxxP motif (*122*), active-site tether (*57*), turn motif, and hydrophobic motif. Sequences are stratified by taxonomic clades across the *y* axis: opisthokonta (animals, fungi, and yeast), viridiplantae (terrestrial and aquatic plants), SAR (protozoa), amoebozoa (protozoa), and excavata (protozoa). Within each clade, sequences are further stratified by conservation of the TIM-Thr (top row). Pie charts (right) show the composition of AGC families within strata. AGC families accounting for less than 10% of each stratum are not shown.

preference that was lost upon mTOR inhibition (fig. S9C). PDK1 binds AGC kinases through a polyvalent interaction with the active-site tether and hydrophobic motif in the C-tail (*65*); however, the ability of PDK1 to bind to PKC C-tail peptides was independent of phosphorylation or phosphomimetic mutations at the TIM (T634E) or turn motif (T641E) sites as assessed by peptide array (fig. S9, D to F).
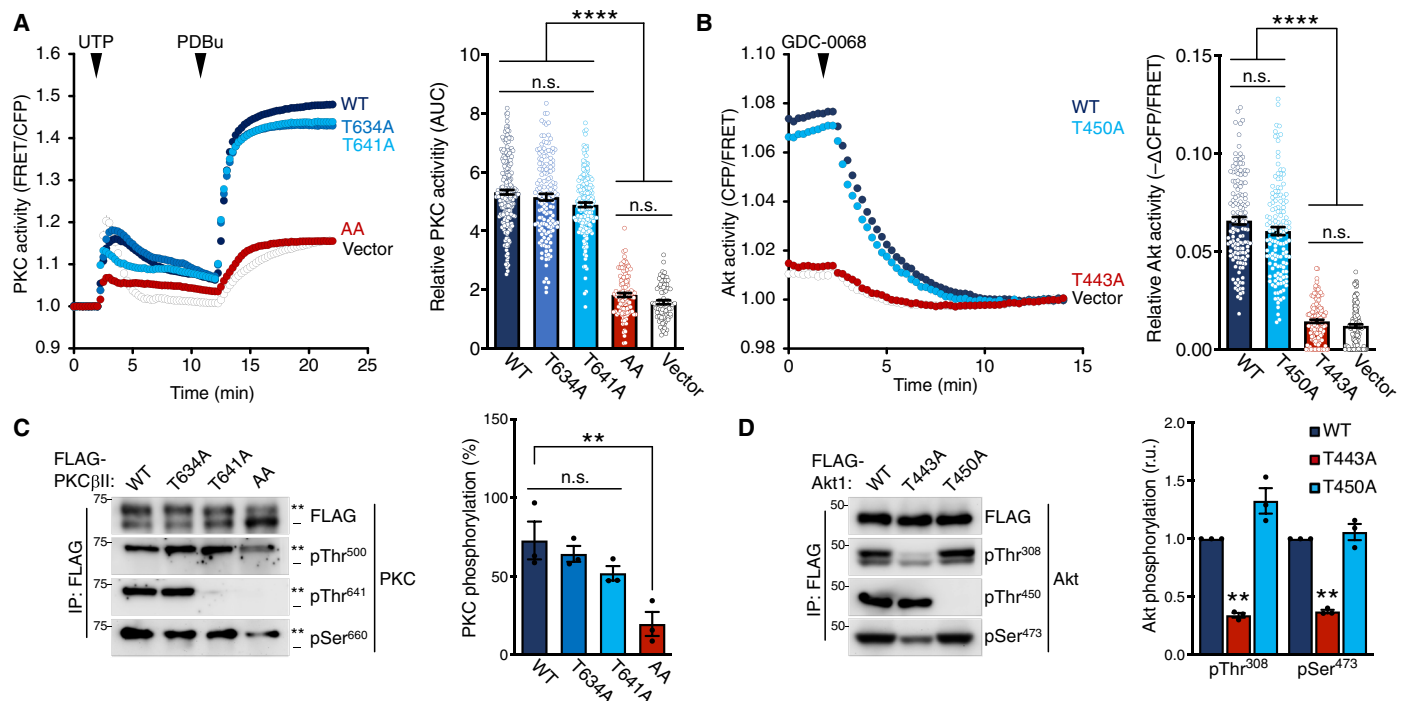
Fig. 5. TIM phosphorylation is critical for PKC and Akt activity. (**A**) PKC activity in COS7 cells expressing CKAR2 (*48*) alone or with mCherry-PKCβII WT, T634A, T641A, or T634A/T641A (AA) and treated with UTP (100 μM) and then PDBu (200 nM) at the times noted. Data represent the normalized FRET ratio changes (means ± SEM) from three independent experiments. Right: Quantification of PKC activity represents the normalized AUC from baseline of 1.0 (means ± SEM) for 20 min after UTP addition. Each data point reflects AUC of single cells from three independent experiments. (**B**) Akt activity in COS7 cells expressing BKAR and mCherry-mAkt1 kinase domain (amino acid residues 141 to 480) WT, T450A, or T443A and treated with the Akt inhibitor GDC-0068 (20 μM). The drop in FRET upon inhibitor addition indicates the degree of basal activity of the isolated kinase domain. Data represent the normalized FRET ratio changes (means ± SEM) from three independent experiments. Right: Quantification of basal Akt activity measured by magnitude of the FRET change (means ± SEM) 12 min after inhibitor addition. Each data point reflects the AUC for a single cell from three independent experiments. (**C**) Western blot of FLAG immunoprecipitates from Triton-solubilized lysates of HEK293T cells expressing FLAG-PKCβII WT, T634A, T641A, or T634A/T641A (AA) and probed with the indicated antibodies. Right: Quantification of PKC phosphorylation (means ± SEM) from three independent experiments represents the percent of the slower-mobility, phosphorylated species (**) over total PKC. Blots are representative of three independent experiments. (**D**) Western blot of FLAG immunoprecipitates from Triton-solubilized lysates of HEK293T cells expressing FLAG-Akt1 catalytic domain (amino acids 141 to 480) WT, T443A, or T450A constructs and probed with the indicated antibodies. Right: Quantification of Akt phosphorylation (means ± SEM) from three independent experiments reflects the normalized phospho-signal for the activation loop (pThr^{308}) or hydrophobic motif (pSer^{473}) relative to total Akt. Blots are representative of three independent experiments. **P < 0.01 and ****P < 0.0001 by one-way ANOVA and Tukey post hoc test or Student's *t* test. n.s., not significant. Western blot quantifications represent the means ± SEM from at least three independent experiments.

Competition with PDK1-interacting fragment (PIF) peptide, which binds to the PDK1 hydrophobic docking site (PIF pocket) with high affinity (*66*, *67*), suppressed the fraction of phosphorylated PKC in the presence or absence of mTOR inhibition as indicated by electrophoretic mobility (fig. S9G). This finding suggests that mTOR regulation of PDK1 binding is mediated through the hydrophobic motif binding site and is regulated at the level of C-tail accessibility, rather than by altered binding affinity upon phosphorylation. This result supports our previous finding, which shows that although PDK1 exhibits higher affinity for phosphorylated hydrophobic motif peptide, PDK1 preferentially associates with unphosphorylated PKC in cells due to increased accessibility of the C-tail in the unphosphorylated state (*68*).

We next assessed the role of TIM and turn motif phosphorylation on kinase domain conformational dynamics with the live-cell reporter KinCon (fig. S10A) (*69*, *70*). This bioluminescence-based reporter uses the protein-fragment complementation luciferase to characterize kinase conformational states in response to various stimuli. TIM/turn motif mutation in PKCβII (T634A/T641A) was

sufficient to alter kinase dynamics (fig. S10B), as assessed by reduced complementation of the split luciferase at N and C termini of the kinase. Mutation of the corresponding residues in S6K1 (T387A/T394A), an mTORC1 substrate, also resulted in a reduction in bioluminescence (fig. S10C), indicating that these residues may serve similar functions in each kinase despite regulation by different TOR complexes. The reduced bioluminescence observed upon mutation of the C-tail phosphorylation sites reflects reduced interaction between the unstructured PKC N and C termini, suggesting that docking of the N-term pseudosubstrate in the active-site cleft and packing of the C-tail against the kinase domain, respectively, may be impaired. However, mutation of the TIM-Thr to acidic residues (T387D/T394D or T387E/T394E) restored complementation to that of WT for S6K1 (fig. S10C), indicating the ability of acidic residues to serve as phosphomimetics for this kinase. Conversely, Glu or Asp substitutions in PKC (T634D/T641D and T634E/T641E) did not rescue bioluminescence to WT levels, reflecting the inability for acidic residues to effectively recapitulate phosphorylation events in some proteins and positions (fig. S10B). For example, Glu at the

PKC activation loop phosphorylation site (T500E) can produce an active PKC, whereas Asp (T500D) cannot (*15*). In the case of TIM, mutation to Ala or Glu abolishes maturation and activation of PKC. Glu at the hydrophobic motif is sufficient for activity, but Glu at the hydrophobic motif itself is not sufficient to rescue activity in the absence of an intact TIM or mTOR activity, indicating that PDK1 phosphorylation and some negative charge on the hydrophobic motif are the two critical requirements for PKC maturation, achieved by mTOR/TIM-mediated recruitment of PDK1. Thus, these findings provide evidence that phosphorylation of the segment comprising the TIM and turn motif dominantly controls PKC activity by altering accessibility of the C-tail to facilitate activation loop phosphorylation by PDK1.

The TIM coordinates PKC dimerization

To explore how TIM phosphorylation by mTORC2 alters C-tail accessibility, we reanalyzed a PKCβII structure of the isolated catalytic domain, in which the active-site tether is resolved (*58*). Examination of the crystal packing revealed a symmetrical, head-to-head PKC homodimer, forming a dimerization interface through hydrophobic interactions in the novel α helix (*58*) that contains the TIM (TIM helix) (Fig. 6A). To determine whether mTOR regulates PKC dimerization in a cellular context, we performed coimmunoprecipitation assays between differentially tagged PKC proteins. Whereas little association of WT PKCβII proteins was observed in untreated cells in which the majority of PKC was in the mature form, mTOR inhibition or TIM/turn mutation (PKCβII AA) enhanced PKC self-association, consistent with dimerization (Fig. 6B). The coimmunoprecipitated PKC was devoid of phosphorylation at the hydrophobic motif (Fig. 6B), indicating that association occurred only between unphosphorylated PKC molecules. Torin treatment resulted in decreased steady-state levels of WT PKC, but not of PKCβII AA, because the unphosphorylated species is unstable. Furthermore, the isolated PKC catalytic domain showed enhanced self-association compared to full-length PKC (fig. S11), suggesting that the PKC regulatory domain impairs dimerization, perhaps by occluding the dimerization interface in the mature form.

To further interrogate PKC self-association in a cellular system, we used a luciferase-based protein-fragment complementation assay (PCA) that has been successfully used to detect protein dimerization in intact cells (Fig. 6C) (*71*). Using this system, we observed a robust association of PKC molecules by PCA, suggestive of steady-state PKC dimerization (Fig. 6D), which was modestly enhanced by TIM/turn motif mutation (AA) (Fig. 6E). Dimerization of TIM/turn motif mutant PKC was more pronounced when protein synthesis was inhibited for 6 hours before the assay (Fig. 6E, +CHX). When overexpressed, some unphosphorylated WT PKC accumulates in cells, which may result in higher baseline dimerization of unprocessed PKC. Thus, inhibiting protein synthesis presumably increases the proportion of phosphorylated WT PKC by allowing sufficient time for the unphosphorylated and unstable protein (*46*) to become phosphorylated or degraded. Because mature (phosphorylated) PKC was monomeric as demonstrated by coimmunoprecipitation (Fig. 6B), reducing the amount of unprocessed WT PKC increased the effect of the PKC AA mutation. Therefore, the TIM/turn motif mutant PKC (AA), which remained unphosphorylated, showed enhanced dimerization compared to phosphorylated WT PKC (Fig. 6E). We next assessed whether PKC dimers could dynamically assemble in cells. In a competition assay, increasing amounts of FLAG-PKCβII was sufficient to displace the PCA protein-protein interaction in a

dose-dependent manner (Fig. 6F), indicating that PKC dimerization is a dynamic association. Furthermore, the ability to dissociate the interaction by competition is consistent with protein dimerization rather than aggregation accounting for the complementation of the split luciferase probes (*72*). The TIM/turn motif mutant PKCβII (AA) more effectively competed with PCA dimerization than did WT PKCβII (Fig. 6F), supporting the preferential dimerization of unprocessed PKC. Furthermore, this finding suggest that TIM/turn motif phosphorylation controls the formation of PKC dimers. In summary, these data are consistent with nascent, unphosphorylated PKC forming a dimer that is disrupted by phosphorylation of the TIM and turn motif.

Because mTORC2 phosphorylation of the TIM promotes hydrophobic motif phosphorylation and also dissociates PKC dimers, we next addressed whether disrupting PKC dimerization would be sufficient to enhance PKC phosphorylation at the hydrophobic motif. To test this possibility, we designed cell-permeable α-helical stapled peptides (*73*, *74*) targeting the TIM to relieve dimerization (Fig. 6G). Treatment of cells overexpressing PKCβII with either of two different PKC dimerization disruptor stapled peptides (S1 and S2) resulted in increased levels of PKC phosphorylation compared to dimethyl sulfoxide (DMSO)–treated controls (Fig. 6H). Although direct binding of the peptides to PKC was not assessed, these data suggest that peptides targeting the TIM designed to disrupt the dimer interface effectively promoted PKC processing. These data are consistent with a model in which the TIM helix coordinates an immature PKC homodimer, which is dissociated by mTORC2 phosphorylation to promote PKC maturation. Moreover, the TIM dimerization interface, previously identified as a novel α helix in the original crystal structure, can be targeted with stapled peptides in cells to induce PKC processing and may be therapeutically actionable.

DISCUSSION

The requirement of mTORC2 for both PKC and Akt hydrophobic motif phosphorylation has been long established, yet the mechanism of this regulation has remained elusive. In this study, we present evidence that mTORC2 performs the first and rate-limiting step of PKC maturation by phosphorylating the newly identified TIM (Fig. 7A), which ultimately facilitates hydrophobic motif autophosphorylation. This regulation by mTORC2 is accomplished by recognition of determinants in the C-tail active-site tether and hydrophobic motif that confer binding to the unprimed (immature, unphosphorylated, and dimerized) PKC species. Dissociation of the PKC dimer upon TIM phosphorylation (Fig. 7B) recruits PDK1 to the unphosphorylated hydrophobic motif to promote activation loop phosphorylation (Fig. 7C). For Akt, activation loop phosphorylation is sufficient to activate the kinase. However, for PKC, this site alone does not enable phosphorylation of downstream substrates but may provide the low rate of catalytic activity required to autophosphorylate the hydrophobic motif (Fig. 7D). After hydrophobic motif phosphorylation, the final step of PKC maturation is autoinhibition by the pseudosubstrate to yield the primed (catalytically competent and stable) PKC species (Fig. 7E) (*46*). This process serves the interdependent functions of stabilizing the catalytically competent and phosphorylated PKC, as well as preventing self-association of the mature form. Moreover, this study identified the TIM as the biological target of the mTOR kinase and provides a mechanism for AGC kinase regulation by mTOR. Thus, our findings establish that the PKC and Akt hydrophobic motif sites, similar to autoregulatory
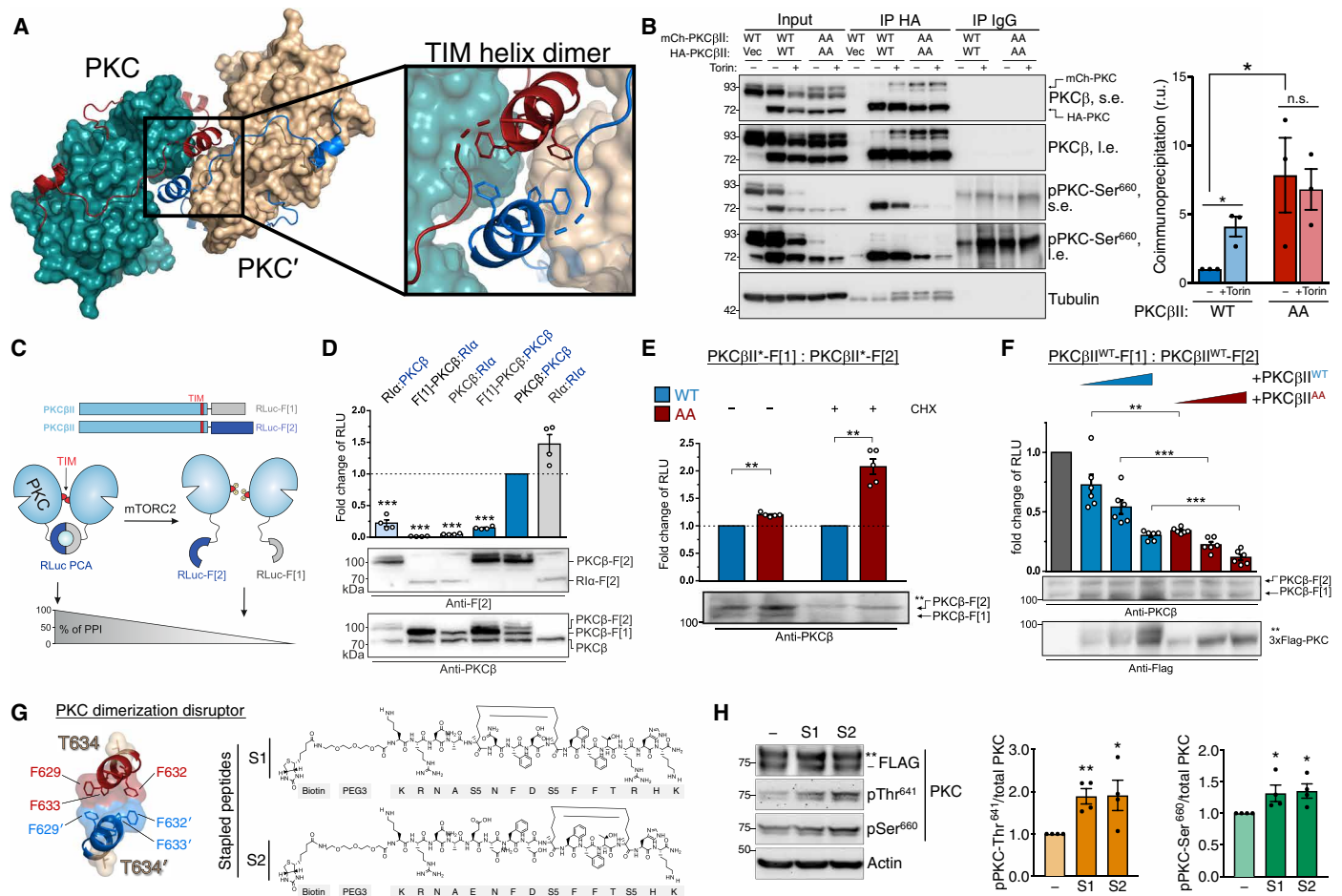
Fig. 6. The TIM coordinates PKC dimerization. (**A**) PKC dimer from PKCβII x-ray structure (PDB ID: 2I0E) showing the PKC kinase (teal) and C-tail (red) with dimer partner (PKC′) kinase (tan) and C-tail (blue). The dimerization interface at the TIM helix is shown with interacting Phe residues. (**B**) Western blot of Triton-solubilized lysates (input) and HA or IgG control immunoprecipitates from HEK293T cells expressing HA- and mCherry (mCh)–PKCβII WT or T634A/T641A (AA) and probed with the indicated antibodies. s.e., short exposure; l.e., long exposure. Right: Quantification of immunoprecipitated mCherry-PKC normalized to the input mCherry-PKC (means ± SEM) from three independent experiments. (**C**) Domain organization of PKCβII constructs tagged with the Renilla luciferase (Rluc)–based PCA fragments Rluc-F[1] and Rluc-F[2]. Scheme illustrates an involvement of the PKC TIM in PKC dimer formation analyzed using the PCA system. PKC dimerization induces the complementation of Rluc fragments and bioluminescent signal reflects the indicated protein-protein interactions (PPI). (**D**) The indicated C-terminally tagged Rluc PCA reporter constructs were transiently coexpressed in HEK293 cells (the exception is the N-terminally tagged F[1]-PKCβ). Data are presented as the fold change in bioluminescent signals [relative light units (RLU)] relative to PKCβII homodimer formation. Each point represents the mean value of an individual experiment performed at least in triplicate; bars indicate the means ± SEM from four independent experiments. ***$P < 0.001$ by Student's t test. The PKA subunit RIα was used as a dimerization positive control. (**E**) PKC dimer formation of PKCβII WT and T634A/T641A (AA), measured in the presence or absence of CHX (250 μM for 6 hours), assessed by the Rluc PCA reporter assay as in (D). Data are presented as the fold change of the PPI signal relative to the WT PKCβII dimer signal. Each point represents the mean value of an individual experiment performed at least in triplicate; bars indicate the means ± SEM from five independent experiments. **$P < 0.01$ by Student's t test. (**F**) Effect of increasing expression of FLAG-PKCβII WT or T634A/T641A (AA) on dimer formation of PKCβII-Rluc-F[1] and PKCβII-Rluc-F[2]. Data are presented as the fold change of the PPI signal in relation to the mock control. Each point represents the mean value of an individual experiment performed at least in triplicate; bars indicate the means ± SEM from six independent experiments. **$P < 0.01$ and ***$P < 0.001$ by Student's t test. (**G**) Dimerization interface of the TIM helix showing hydrophobic interactions and TIM phosphorylation site (Thr^{634}). Kekulé structures of two PKC dimerization disruptor (PKC-DD) stapled peptides targeting the TIM. (**H**) Western blot of HEK293T cells expressing FLAG-PKCβII, treated with 10 μM of the indicated PKC-DD stapled peptides for 24 hours before lysis, and probed with the indicated antibodies. Right: Quantification represents the amount of PKC phosphorylated at Thr^{641} or Ser^{660} normalized to total PKC from three independent experiments. *$P < 0.05$ and **$P < 0.01$ by Student's t test or one-way ANOVA. Error bars represent SEM from at least $n = 3$ experiments.

sites in the C-terminal tail of receptor tyrosine kinases (*75*), are regulated by autophosphorylation (Fig. 8).

Characterization of TIM phosphorylation may have been hindered by the potentially transient nature of phosphorylation at this site, as evidenced by the low rate of identification in proteomic studies (*62*). First detected by MS as a PKC phosphorylation event in insect cell

expression (*76*), TIM phosphorylation may be more sensitive to phosphatases because of its outward orientation on an exposed segment of the C-tail. TIM phosphorylation was previously detected as a "protected" PKC phosphorylation in neurons during long-term potentiation. In this study, we detected PKC TIM phosphorylation by MS in mouse brain, suggesting that stable phosphorylation at the
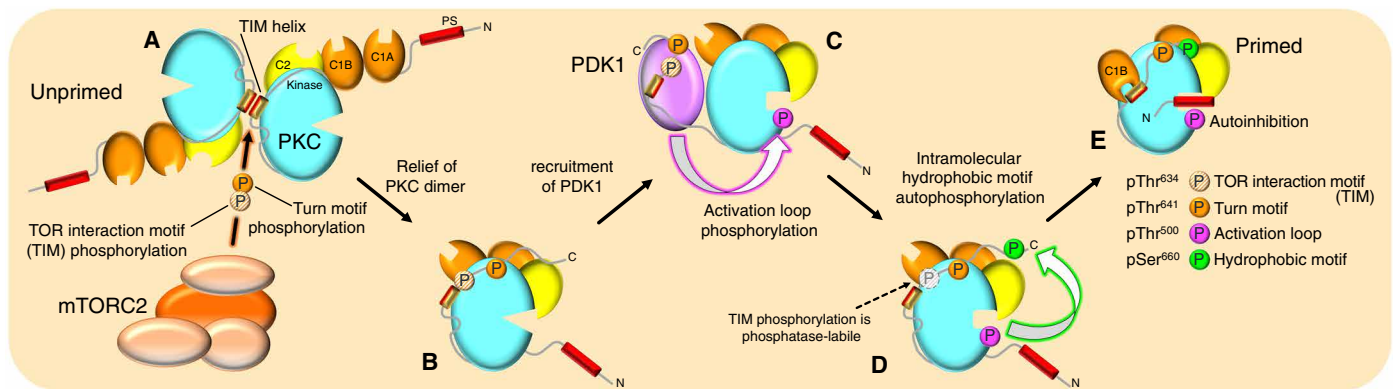
Fig. 7. Model of PKC maturation by phosphorylation. (**A**) Newly synthesized PKC exists as a homodimer mediated by the TIM helix, with membrane targeting domains exposed, and is neither phosphorylated nor catalytically active (unprimed). (**B**) mTORC2 binds to disrupt the dimer interface and phosphorylates the TIM and turn motif to relieve the PKC dimer, exposing the C-terminal tail to recruit PDK1. (**C**) Bound PDK1 phosphorylates PKC at the activation loop. (**D**) Activation loop phosphorylation triggers intramolecular autophosphorylation at the hydrophobic motif. (**E**) Phosphorylation at the hydrophobic motif triggers binding of the pseudosubstrate to the substrate binding cavity to affect autoinhibition (primed). This species of PKC, which is stable and catalytically competent, is maintained in an inactive state by the pseudo-substrate, poised for activation by the second-messenger diacylglycerol and Ca^{2+}.
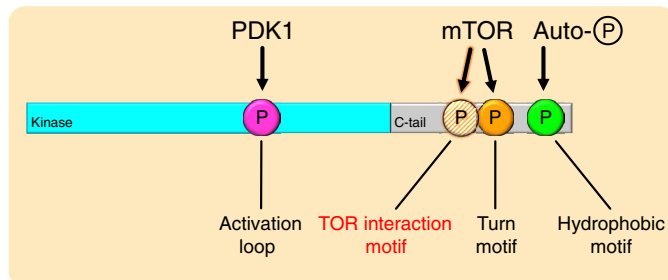
Fig. 8. Model for phosphorylation of mTOR-regulated AGC kinases. mTOR-regulated kinases are phosphorylated at the activation loop, turn motif, hydrophobic motif, and the newly identified TIM. The TIM and turn motif are phosphorylated by mTOR, which facilitates activation loop phosphorylation by PDK1 and triggers hydrophobic motif autophosphorylation to activate the kinase.

TIM site exists in certain phosphatase environments. The critical role for TIM phosphorylation specifically during PKC processing and compensation by the turn motif phosphorylation suggests that this site may only be required in the recruitment of PDK1 and is dispensable thereafter. Whether this phosphorylation plays a more dynamic role in kinases such as Akt that are transiently activated by PDK1 merits further investigation.

The turn motif phosphorylation, which is the constitutive and stable mTOR phosphorylation, may additionally confer the ability to autophosphorylate the hydrophobic motif. In support of this notion, mature PKC that is dephosphorylated at the activation loop and hydrophobic motif in vitro but retains the turn motif phosphorylation autophosphorylates the hydrophobic motif (7). However, dephosphorylation of the turn motif site abolishes PKC reautophosphorylation, which is rescued by incubation with catalytically competent PDK1 (6). Therefore, turn motif phosphorylation may lock into place the conformational changes conferred by activation loop phosphorylation, facilitating PDK1-independent reautophosphorylation that extends the signaling lifetime of PKC (77). Furthermore, we showed here that TIM phosphorylation and turn motif phosphorylation compensated for one another in PKC, but the TIM site

was dominant in Akt. The turn motif does not directly regulate the activity of PKC, Akt, or PKA in vitro but instead anchors the C-tail to the kinase domain to stabilize AGC kinases (65). Even in the case of PKA, which has a divergent turn motif site that is mTORC2 independent, phosphorylation of the turn motif is a prerequisite for activation loop phosphorylation in cells (78). Thus, phosphorylation of the TIM and/or turn motif sites may coordinately facilitate the initial activation by PDK1 in multiple AGC kinases and sustain a regulatory "memory" of activation. That the TIM is more highly conserved than the turn motif in eukaryotic kinases across evolution supports our conclusion that the TIM is the primary target of mTOR and the basis of mTORC2 regulation for a subset of AGC kinases.

Elucidating the hydrophobic motif as an mTORC2-facilitated and PDK1-dependent autophosphorylation highlights the intricate regulation of AGC kinase activation. PKC hydrophobic motif phosphorylation, which occurs during priming, is essential for its catalytic activity in cells, whereas this acutely regulated site in Akt tunes its activity. For some AGC kinases, however, hydrophobic motif phosphorylation occurs first to create a docking site for PDK1 (3). In all cases, activation loop phosphorylation is the critical event for activation, and this process appears to be regulated principally by PDK1 recruitment, which is achieved by a multitude of mechanisms (79). That PDK1-dependent activation is regulated at the level of binding is expected, because PDK1 is present at low nanomolar concentrations, whereas its substrates may outnumber that by as many as two orders of magnitude in the cell (80). In addition, PDK1 lacks a canonical AGC kinase C-tail and requires the transinteracting C-tail of the recipient kinase for activation. The PDK1 C-tail sequence diverges immediately preceding the TIM (57), suggesting that binding this regulatory element, such as the hydrophobic motif, directs PDK1 activity and specificity toward its substrates. Thus, recruitment of PDK1 to the C-tail is the rate-determining step of PKC maturation, regulated by mTORC2 phosphorylation of the TIM, and is likely the limiting factor in AGC kinase activation. The TIM is also conserved in S6K1 and S6K2, which are regulated by mTORC1. A unique C-terminal extension in S6K precludes regulation by mTORC2 (81), and the hydrophobic motif is instead modified by mTORC1 through a distinct TOR signaling motif (82). A study reporting the

S6K hydrophobic motif as an autophosphorylation target (*83*) raise the interesting possibility that TIM phosphorylation by mTORC1 may serve a similar function in S6K activation by recruiting PDK1 (*84*) but is subject to regulation by the multitude of nutrient-sensing inputs that feed into mTORC1 (*85*). Furthermore, the TIM is present in RSK family kinases, which are mTORC2-regulated kinases (*37*), and MSK family kinases, which are not known to be regulated by mTOR (*86*). Establishing the specific role of TIM phosphorylation in distinct kinase families awaits future studies.

The ability to regulate function by autophosphorylation is a prevalent theme in kinase biology (*87*). In general, conformational switches convert kinases into a mode "prone to autophosphorylation," which allows stabilizing or activating autophosphorylation. In vitro studies with purified PKC have shown that the enzyme autophosphorylates by an intramolecular reaction at C-terminal sites including the hydrophobic motif (*76*, *88*). Furthermore, purified enzyme selectively dephosphorylated at this site in vitro can reincorporate phosphate at that position in a concentration-independent manner (*7*, *31*, *89*). The inability of kinase-inactive constructs to incorporate phosphate at the hydrophobic motif in cells supports the notion that this site is cis-autophosphorylated (*31*, *46*). This finding has been refuted in a study showing that active-site inhibitors allow phosphate accumulation of the hydrophobic motif on kinase-inactive constructs (*90*). However, occupancy of the active site by inhibitors or peptide substrates prevents PKC dephosphorylation, and mutants that have weak activity accumulate phosphate at this site (*46*, *50*). In the case of Akt, multiple mechanisms have been proposed to control the phosphorylation of the hydrophobic motif (*91*). However, as for PKC, Akt activation loop phosphorylation by PDK1 triggers hydrophobic motif phosphorylation of active Akt, but not the inactive form (*30*). Furthermore, phosphorylation of the hydrophobic motif is impaired in kdAkt (*14*, *30*, *33*). The discovery that the mTOR kinase promotes hydrophobic motif phosphorylation for several AGC kinases has confounded a consensus on the mechanism of regulation at this site. Our current study resolves this question by showing that mTORC2 "primes" PKC for activation loop phosphorylation by the critical kinase, PDK1, with the immediate consequence being autophosphorylation of the hydrophobic motif. Thus, mTORC2 facilitates the PDK1 step that converts PKC into an "autophosphorylation-prone" conformation.

An unexpected finding from this study is the ability of immature PKC to homodimerize. Specifically, coimmunoprecipitation and protein complementation studies revealed a TIM-dependent association of PKC molecules. Additional biophysical and structural analyses to better define the complex will be important. Dimerization of mature PKC has previously been proposed in vitro in the presence of Ca^{2+} and phosphatidylserine or in cells upon activation (*92*, *93*); however, these studies do not take into account the reduction in dimensionality upon PKC engagement on a lipid membrane or vesicle and may have limited biological relevance. Instead, biophysical studies support mature (phosphorylated) PKC functioning as a monomer in cells (*94*). In addition, biochemical studies reveal that the purified mature PKC is monomeric even when bound to activating lipid surfaces (*95*), where it autophosphorylates in a concentration-independent manner, indicative of monomeric function (*88*). Consistent with the activated form being unlikely to dimerize, the C2-mediated translocation of PKCβII is a diffusion-driven process (*96*) and relies upon intramolecular, rather than intermolecular, contacts with the kinase domain (*97*). Thus, our finding in this study that newly synthesized PKC exists as an immature homodimer regulated by mTORC2-mediated

TIM phosphorylation is likely to be the only biologically relevant dimer that is consistent with PKC biochemistry. Akt has been proposed to dimerize (*98*, *99*); however, whether mTORC2-mediated TIM phosphorylation also regulates Akt dimerization or relieves PH domain autoinhibition to facilitate its activation remains to be determined.

Strategies to manipulate hydrophobic motif phosphorylation may be applicable in therapies for cancer, in which this site is frequently dysregulated. The AGC kinase hydrophobic motif is a hotspot for cancer-associated mutations in sites of posttranslational modifications (*100*). In addition, PKC quality control, which involves PHLPP-mediated hydrophobic motif dephosphorylation and degradation, is exploited by cancer cells to suppress PKC protein levels (*26*, *46*). Thus, maintaining the integrity of the PKC processing machinery that permits hydrophobic motif phosphorylation is critical for PKC's tumor-suppressive function (*101*, *102*). Conversely, Akt hydrophobic motif phosphorylation generally serves an oncogenic role, and constitutively active or amplified Akt is prevalent in many cancers that frequently harbor phosphatidylinositol 3-kinase pathway alterations (*103*). In these cancers, mTOR is an attractive therapeutic target (*104*); however, this strategy should be approached with caution because mTORC1/2 inhibitors would have the unwanted consequence of inhibiting PKC processing, depleting the levels of an important tumor suppressor. Therefore, the efficacy of mTOR therapies could be potentiated by third-generation mTOR inhibitors that selectively target mTORC1 (*105*) or by methods to promote mTOR-independent PKC processing, such as by targeting PKC dimerization with stapled peptides as we have performed here.

In summary, our study reveals the long-elusive role of mTORC2 in PKC regulation: This kinase complex binds to and phosphorylates a previously unidentified TIM to facilitate the critical binding of PDK1 to the C-terminal tail of newly synthesized PKC, thus initiating the maturation of the enzyme to the fully phosphorylated and catalytically competent state. Our work detailing the molecular basis of PKC and Akt regulation by mTORC2 provides new lines of investigation into the mechanisms of AGC kinase activation. Understanding the determinants for signal propagation through these kinases will facilitate the identification of new therapeutic strategies to modulate diverse cellular processes and disease states.

MATERIALS AND METHODS
Cell culture and transfection
WT, $Ric^{-/-}$, and $Sin1^{-/-}$ MEFs were previously described (*40*). MEFs, COS7, and human embryonic kidney (HEK) 293T cells were cultured in Dulbecco's modified Eagle's medium (DMEM) (Corning) containing 10% fetal bovine serum (FBS) (Atlanta Biologicals) and 1% penicillin/streptomycin (Gibco) at 37°C in 5% CO_2. Transient transfection was carried out using the Lipofectamine 3000 Transfection Reagent (Thermo Fisher Scientific). Cells used were periodically tested for *Mycoplasma* contamination using a polymerase chain reaction (PCR)–based protocol (*106*) and showed no evidence of contamination.

Comparative sequence analysis
An alignment profile of the C-tails in human AGC kinases was created starting from the PxxP motif to the hydrophobic motif. The profile was expanded with iterative BLASTp (*107*) searches on UniProtKB until convergence and aligned using MAFFT v7.310 (*108*). Members of the AGC kinase group were identified from UniProt proteomes (retrieved 9 October 2019) using MAPGAPS (*109*). From this filtered set,

we identified and aligned AGC C-tails with the aforementioned profile using MAPGAPS (*109*). Kinase domains residing N terminus to the AGC C-tails were classified according to AGC families defined by the manning classification (*110*) using MAPGAPS (*109*). Sequence taxonomy was determined by mapping UniProt OX values to National Center for Biotechnology Information taxdump (retrieved 23 March 2019). Phosphorylation sites were mapped using PhosphoSitePlus (*62*). Sequence logos were created using WebLogo 3 (*111*).

FRET imaging and analysis

Cells were imaged as described previously (*112*). For activity experiments, MEFs and COS7 cells were cotransfected with the indicated mCherry-tagged PKC construct and CKAR or CKAR2. For Kinameleon experiments, the indicated Kinameleon construct containing monomeric yellow fluorescent protein (mYFP) and monomeric cyan fluorescent protein (mCFP) was transfected alone. For translocation experiments, MEFs cells were cotransfected with the indicated mYFP-tagged construct and plasma membrane–targeted mCFP. Baseline images were acquired every 15 s for 2 min before drug addition. FRET ratios represent the means ± SEM from at least three independent experiments. FRET ratios (FRET/CFP or CFP/FRET) were standardized such that greater values corresponded to increased phosphorylation of the reporter, indicative of increased kinase activity. All data were normalized to the baseline FRET ratio of each individual cell unless otherwise noted; in some cases, the absolute FRET ratio was plotted, or traces were normalized to levels after inhibitor addition. Area under the curve (AUC) represents means ± SEM of individual cells from the time of the first drug addition ($t = 2$ min) until the indicated time point, integrated over the normalized initial value $y = 1$. When comparing translocation kinetics, data were also normalized to the maximal amplitude of translocation for each cell, as previously described (*51*), to compare translocation rates. This normalization was performed because the maximal amplitude of translocation of the mutants varied, possibly because of changes in the orientation or distance of the fluorophores caused by differential folding of the mutant kinases.

Immunoblotting and antibodies

Cells were lysed in potassium phosphate buffer (PPHB): 50 mM NaPO$_4$ (pH 7.5), 1% Triton X-100, 20 mM NaF, 1 mM Na$_4$P$_2$O$_7$, 100 mM NaCl, 2 mM EDTA, 2 mM EGTA, 1 mM Na$_3$VO$_4$, 1 mM phenylmethylsulfonyl fluoride (PMSF), leupeptin (40 mg/ml), 1 mM dithiothreitol (DTT), and 1 mM microcystin. Whole-cell lysates were sonicated, Triton-solubilized lysates were centrifuged at 13,000g for 3 min, and supernatant was isolated. Lysates were analyzed by SDS–polyacrylamide gel electrophoresis (PAGE), transferred to polyvinylidene difluoride (PVDF) membrane (Bio-Rad), blocked in 5% nonfat dry milk for 1 hour at room temperature, incubated with primary antibodies at 1:1000 dilution overnight at 4°C, incubated with horseradish peroxidase (HRP)–conjugated secondary antibody at 1:10,000 dilution for 1 hour at room temperature, and detected using chemiluminescence SuperSignal West reagent (Thermo Fisher Scientific) on a FluorChem Q imaging system (ProteinSimple). Blots were washed three times with 1× Tris-buffered saline, 0.1% Tween 20 (TBST) between incubations. The pan anti–phospho-PKC activation loop antibody (PKC pThr^{500}) (*6*) and TIM antibody (PKC pThr^{634}) (*61*) were described previously. The anti–phospho-PKCα/βII turn motif (pThr$^{638/641}$; 9375S), anti-PKCδ/θ turn motif (9376S), anti-Myc (D84C12), anti-mTOR (7C10), anti-Rictor (53A2), anti-Raptor

(24C12), anti-S6K (9202S), anti-pS6K Thr^{389} (9205), anti-PDK1 (3062S), anti–phospho-PKN1/PKN2 activation loop antibody (2611), anti-vinculin (4650S), anti–phospho-Akt pThr^{308} (244F9)/pT450 (D5G4)/pSer^{473} (D9E), pan anti–phospho-PKC hydrophobic motif (βII pSer^{660}; 9371S), and anti–phospho-Thr (clone 42H4; 9386S) antibodies were purchased from Cell Signaling Technologies. The anti-Sin1 antibody was from Abcam (ab71152). Anti-PKCβ antibody was purchased from BD Transduction Laboratories (610128). The anti-DsRED antibody was purchased from Clontech. The anti–glutathione *S*-transferase (GST) (clone B-14; sc-138) and rabbit (sc-2491) and mouse (H-270; sc-66931) immunoglobulin G (IgG) antibodies were purchased from Santa Cruz Biotechnology. The anti-hemagglutinin (HA) antibody for immunoblot was purchased from Roche. The anti-HA (clone 16B12; 901515) and anti-FLAG (clone L5; 637301) antibodies used for immunoprecipitation were purchased from BioLegend. The anti–α-tubulin (T6074) antibody, anti-FLAG antibody for immunoblot (clone M2; F1804), and the anti–β-actin antibody (A228) were from Sigma-Aldrich. PCA lysates were probed with mouse anti–Renilla luciferase (Rluc) antibody (Chemi-Con, #MAB4400) against Rluc-F[2]. HRP-conjugated anti-mouse (7076), anti-rabbit (7074), and anti-rat (7077) secondary antibodies were from Cell Signaling Technologies. Gö6976 (*113*), Gö6983 (*114*), PDBu, UTP, CHX, Torin1, and Calyculin A were purchased from Calbiochem. GDC-0068 (S2808) (*115*) was purchased from Selleck Chemicals.

In vitro kinase assays

In vitro kinase assays were performed similarly to mTOR kinase assays as described previously (*27*, *116*). Briefly, for the mTORC2 kinase assays experiments, because of poor stability of mTORC2 complex, kinase assays were performed on the same day of the isolation of the complex. After 48-hour transfection of HEK293T cells with the HA-Sin1 plasmid, cells were lysed in CHAPS buffer [40 mM Hepes (pH 7.4), 120 mM NaCl, 1 mM EDTA, 0.3% CHAPS, 50 mM NaF, 5 mM sodium pyrophosphate (Na$_4$P$_2$O$_7$), 10 mM sodium glycerol phosphate (C$_3$H$_7$Na$_2$O$_6$P), 1 mM DTT, 1 mM Na$_3$VO$_4$, 1 mM PMSF, leupeptin (50 µg/ml), 1 µM microcystin, and 2 mM benzamidine]. Lysates were incubated for 30 min on ice and centrifuged at 13,000g for 15 min at 4°C. Supernatants were collected and quantified by Bradford assay, and 5 mg of lysate was used per condition. Five milligrams of lysate was incubated with 15 µl of HA beads (Thermo Fisher Scientific, catalog number 26181), previously washed three times with phosphate-buffered saline (PBS), for 1 hour at 4°C in a nutator. Samples were centrifuged at 500g for 5 min at 4°C, and pellets washed six times with CHAPS buffer. Pellets were washed twice with kinase assay buffer [25 mM Hepes (pH 7.4) and 50 mM KCl]. Beads were incubated with 0.5 µg of the GST-tagged C-tails of PKC, and kinase assay was performed for 30 min at 30°C. The conditions of the kinase assay were 25 mM Hepes (pH 7.4), 50 mM KCl, 0.5 µg of substrate protein, 10 mM MgCl, and 250 µM adenosine 5′-triphosphate in a final reaction volume of 25 µl. After the 30-min incubation at 30°C, reactions were stopped by adding 5 µl of sample buffer 4X and boiled at 100°C for 5 min (for Western blot analysis) or by 500g for 5 min to separate the mTORC2 complex from the PKC C-tails (for MS analysis). Reactions were analyzed by SDS-PAGE and immunoblotting as described.

Liquid chromatography–MS analysis

In vitro kinase assays were analyzed by liquid chromatography–MS (LC-MS) as follows. Samples were dried and resuspended in digest

buffer [1 M urea and 50 mM Hepes (pH 8.5)] for digestion with sequencing grade trypsin (Promega; 6 hours at 37°C). Digested peptides were desalted with Sep-Pak (Waters), dried, and resuspended in 5% formic acid/5% acetonitrile for LC-MS analysis. LC-MS analysis was conducted as previously described (117) with the following modifications. Peptides were eluted on a gradient of 85 min, and only MS1 and MS2 scans were taken. Raw files were searched against the human UniProt database (downloaded March 2019) using the Sequest algorithm with a decoy search conducted on sequences in reverse order to filter matches to a false discovery rate of <1%. Mass tolerances were set to 50 parts per million (ppm) for MS1 and 0.6 Da for MS2. Oxidation of methionine and phosphorylation of serine, threonine, and tyrosine were specified as variable modifications. Quantification of phospho-peptides and proteins was based on MS1 AUC. The representative spectrum of PKCβII Thr[634] phosphorylation from mouse brains was derived from a phospho-proteomic dataset. All procedures involving animals were approved by The Scripps Research Institute's Institutional Animal Care and Use Committee and met the guidelines of the National Institutes of Health (NIH) detailed in the *Guide for the Care and Use of Laboratory Animals* (118).

Luciferase PCA analyses

HEK293 cells were grown in DMEM supplemented with 10% FBS. We transiently overexpressed indicated versions of the Rluc-PCA–based reporter in 24-well plate formats. Transient transfections were performed with TransFectin reagent (Bio-Rad, #1703352) according to the manufacturer's instructions. Experiments were performed 48 hours after transfection. For the luciferase-PCA measurements, the growth medium was removed, and cells were washed with PBS. Cell suspensions were transferred to 96-well plates and subjected to luminescence analysis using the PHERAstar FSX (BMG LABTECH). Luciferase luminescence signals were integrated for 10 s after addition of the Rluc substrate benzyl-coelenterazine (NanoLight, #301).

Molecular modeling

Molecular docking of the Sin1 CRIM domain [Protein Data Bank (PDB) ID: 2RVK] (59) and PKCβII (PDB ID: 2I0E) (58) was performed using ClusPro (119) without any restrictions and using the default settings. Structure diagrams were generated with PyMOL (120). Kinome tree (110) plots were generated using Coral (121).

Peptide arrays

Peptide arrays were generated by the INTAVIS MultiPep RS peptide synthesizer (INTAVIS Bioanalytical Instruments AG, Koeln, Germany) using standard 9-fluorenylmethoxycarbonyl (Fmoc) protection–based solid-phase peptide synthesis to produce short, overlapping 15- or 18-mer peptides directly conjugated onto amino–polyethylene glycol (PEG)–modified cellulose membranes (ACS01, Intavis AG). Each peptide spot sequence corresponds to a segment of the rat PKCβII kinase domain and C-terminal tail (296 to 673) by shifting in increments of one or three amino acids. Arrays were vacuum-dried, sealed in plastic, frozen at −20°C, rehydrated in 100% ethanol for 30 min, and washed three times with TBS-T before use. Array strips were blocked with 5% nonfat dry milk in TBS-T (0.0005% Tween 20) for 1 hour at room temperature, overlaid with cell lysate from WT MEFs or HEK293T cells overexpressing Sin1, mTOR, Raptor, or PDK1 for 1 hour, incubated with 1:1000 HA, Myc, or

mTOR primary antibody for 1 hour at room temperature, incubated with 1:5000 HRP-conjugated secondary antibody for 1 hour at room temperature, and developed by immunoblot protocol described above. Arrays were washed three times for 5 min each with TBS-T between each incubation.

Plasmids and constructs

The CKAR (47), CKAR2 (48), and B kinase activity reporter (BKAR) (64) were previously described. mCherry-tagged constructs were cloned into pcDNA3 with mCherry at the N terminus at the Bam HI and Xba I sites. mYFP-tagged constructs were cloned into pcDNA3 with mYFP at the N terminus at the Xho I and Xba I sites. HA-tagged constructs were cloned into pcDNA3 with HA at the N terminus at the Not I and Xba I sites. FLAG-tagged constructs were cloned into pCMV at the N terminus at the Not I and Xba I sites. Kinameleon was cloned into pcDNA3 as mYFP-PKCβII-mCFP. Point mutations were generated by site-directed mutagenesis. GST constructs of the C-terminal tail of PKCβII (601 to 673) with specified mutations (T634A, T641A, S660A, T634E, and T634E/S660A) and GST-PIF were generated as described previously (68). MyrPalm constructs contain N-terminal Lyn kinase (MGCIKSK) sequence. Myr constructs contain the N-terminal Src sequence (MGSSKSKPK). The Rluc-PCA–based hybrid proteins were designed as previously described (72). Briefly, the coding regions of RIα (NP_037313.1) and PKCβII (NP_002729.2); complementary DNA (cDNA) template was provided by G. Baier) were PCR-amplified and cloned into an eukaryotic expression vector and fused either N- or C-terminally with -F[1] or -F[2] of the Rluc-PCA. PKC chimera fusion proteins were generated by cloning the N terminus of mTORC2-independent PKCδ, including the regulatory domains, kinase domain, and various fragments of the C-tail as indicated, to C-terminal fragments of the PKCβII C-tail to create a full-length chimera at various C-tail junctions. Chimeras were cloned pcDNA3 vectors with mCherry tags. An identical approach was used for the PKCθ/β chimera. A site-directed mutagenesis approach was used to generate the T634A/T641A double mutants of PKCβII. The Rluc-PCA–based hybrid proteins F[1]-PKCβII-F[2] and F[1]-S6K1-F[2] (NP_003152.1) were generated using an identical cloning approach as described previously (70). A site-directed mutagenesis approach was used to generate the T634A/T641A, T634D/T641D, and T634E/T641E double mutants of PKCβII as well as the T387A/S394A, T387D/S394D, and T387E/S394E double mutants of S6K. Catalytic domains of murine PKN2 (UniProtID, Q8BWW9; 645 to 983) and PKN1 (UniProtID, P70268; 607 to 946) were cloned into pcDNA3.1/Zeo vector (Thermo Fisher Scientific) with N-terminal FLAG tag. Cloning and mutagenesis were performed using the In-Fusion HD Cloning Kit (Clontech) and verified by sequencing.

Pulse-chase and immunoprecipitation experiments

For pulse-chase experiments, COS7 cells were incubated with Met/Cys-deficient DMEM (Corning) with 10% FBS for 30 min at 37°C. The cells were then pulse-labeled with 0.5 mCi/ml [35S]Met/Cys (PerkinElmer) in Met/Cys-deficient DMEM for 7 min at 37°C, medium was removed, cells were washed with Dulbecco's phosphate-buffered saline (DPBS) (Corning), and cells were chased with DMEM culture medium (Corning) containing 200 mM unlabeled methionine, 200 mM unlabeled cysteine, and 10% FBS. At the indicated times, cells were lysed in PPHB and centrifuged at 13,000g for 3 min at 22°C, supernatants were precleared for 30 min at 4°C with

Protein A/G Beads (Santa Cruz Biotechnology), and protein complexes were immunoprecipitated from the supernatant with 1:100 dilution of either an anti-HA or anti-FLAG monoclonal antibody (BioLegend, 16B12; L5) overnight at 4°C. The immune complexes were collected with Protein A/G Beads (Santa Cruz Biotechnology) for 2 hours at 4°C, washed four times with PPHB, separated by SDS-PAGE, transferred to PVDF membrane (Bio-Rad), and analyzed by autoradiography and Western blot. GST pull-down experiments used a similar approach with glutathione resin (Pierce, 16101) for purification.

Purification of GST-tagged C-tails of PKC for in vitro kinase assays

After 48-hour transfection of HEK293T cells with Effectene (QIAGEN) with the GST-PKCβ C-tail (601 to 673) WT or T634A plasmids, cells were lysed in lysis buffer [20 mM Tris (pH 7.5), 150 mM NaCl, 1 mM EDTA, 1 mM EGTA, 1% Triton X-100, 2.5 mM sodium pyrophosphate ($Na_4P_2O_7$), 1 mM β-glycerol phosphate, 1 mM DTT, 1 mM Na_3VO_4, 1 mM PMSF, leupeptin (50 μg/ml), 1 μM microcystin, and 2 mM benzamidine]. Lysates were incubated for 10 min on ice and centrifuged at 13,000g for 10 min at 4°C. Supernatants were incubated with 65 μl of GST beads (Pierce, 16101) previously washed three times with PBS, for 1 hour at 4°C in a nutator. Samples were centrifuged at 500g for 2 min at 4°C, and pellets washed two times with lysis buffer and two times with elution buffer [50 mM Hepes (pH 7.5), 100 mM NaCl, 5 mM β-glycerol phosphate, 1 mM DTT, 0.01% NP-40, and 10% glycerol]. Beads were incubated with 10 mM glutathione in elution times at 4°C for 15 min, and centrifuged at 500g for 2 min at 4°C, and supernatants were collected. This step was repeated three more times to increase the yield. Purified protein was exchanged into 20 mM Hepes (pH 7.5), 1 mM EDTA, 1 mM EGTA, and 1 mM DTT using 10-kDa Amicon centrifugal filter unit (EMD Millipore). Protein concentration was determined using bovine serum albumin (BSA) standards on an SDS-PAGE gel stained with Coomassie brilliant blue stain.

Stapled peptide experiments

Peptides used in this study were synthesized using Fmoc-protected solid-phase peptide synthesis on Rink Amide MBHA resin. Synthesis was performed in NMP (1-methyl-2-pyrrolidinone). Deprotection was performed using 25% (v/v) solution of piperidine in NMP for 30 min. Amino acid coupling was carried out by adding 10 equivalents of Fmoc-protected amino acid (0.25 M final concentration) along with HCTU [O-(1H-6-chlorobenzotriazole-1-yl)-1,1,3,3-tetramethyluronium hexafluorophosphate] in NMP (0.24 M final concentration), followed by 8% (v/v) DIEA (N,N-diisopropylethylamine) for 45 min. The olefinic amino acid S 5 [Fmoc-(S)-2-(4-pentenyl)alanine] was incorporated as denoted in the sequences below using standard coupling conditions at i, i + 4 positions. Ring closing metathesis was carried out on protected and resin bound peptides using 0.4 equivalents of Grubb's first-generation catalyst [benzylidenebis(tricyclohexylphosphine)dichlororuthenium] in 1,2-dichloroethane for 1 hour. Olefin metathesis was performed twice to ensure completion of staple formation. N-terminal addition of PEG three (Fmoc-11-amino-3,6,9-trioxaundecanoic acid, denoted as asterisks in sequences below) was conducted with 4 M equivalents under standard coupling conditions. Peptides were biotin-labeled at the N terminus using 10 equivalents of D-biotin, 0.14 M HCTU, and 4% (v/v) DIEA in a 1:1 mixture of N,N′-dimethylformamide and DMSO overnight at room temperature. Peptides were cleaved from

resin using 95% trifluoroacetic acid, 2.5% water, and 2.5% triisopropylsilane for 4 hours. Products were then precipitated in ice-cold methyltert-butyl ether and air-dried. Crude products were dissolved in methanol and purified using high-performance LC over a 10 to 100% acetonitrile gradient. Products were verified by mass spectroscopy and quantified by measuring diminished absorbance of 2-(4′-hydroxybenzeneazo)benzoic acid–avidin complex at 500 nm. Molecular weights of the purified products are as follows: S1: Biotin-PEG3-KRNA*NFD*FFTRHK, actual mass of 2345.4 (expected mass of 2345.8); and S2: Biotin-PEG3-KRNAENFD*FFT*HK, actual mass of 2318.2 (expected mass of 2318.7).

Transient transfection of 3XFlag-rPKCβII was carried out using Effectene (QIAGEN) for 24 hours. At the time of transfection, HEK293T cells were treated with vehicle (DMSO) or one of the two stapled peptides (S1 or S2) (10 μM) designed to bind PKC and disrupt its dimerization. Cells were incubated at 37°C in 5% CO_2 for 24 hours and then lysed in 50 mM tris (pH 7.4), 1% Triton X-100, 50 mM NaF, 10 mM $Na_4P_2O_7$, 100 mM NaCl, 5 mM EDTA, 1 mM Na_3VO_4, 1 mM PMSF, leupeptin (50 μg/ml), 1 μM microcystin, and 2 mM benzamidine. Homogenates were sonicated, and protein was quantified using a bicinchoninic acid (BCA) protein assay kit (Thermo Fisher Scientific). Thirty micrograms of protein was separated by standard SDS-PAGE and transferred to PVDF membranes (Bio-Rad). Membranes were blocked with 5% BSA or 5% milk for 1 hour at room temperature and analyzed by immunoblotting with specific antibodies. Detection of immunoreactive bands was performed using chemiluminescence on a FluorChem Q imaging system (Alpha Innotech).

Quantification and statistical analysis

Statistical significance was determined using repeated-measures one-way analysis of variance (ANOVA) and Brown-Forsythe test or Student's t test performed in GraphPad Prism 6.0a (GraphPad Software). The half-time of translocation was calculated by fitting the data to a nonlinear regression using a one-phase exponential association equation with GraphPad Prism 6.0a (GraphPad Software). AUC calculations were performed in GraphPad Prism 6.0a (GraphPad Software). Western blots and autoradiographs were quantified by densitometry using the AlphaView (ProteinSimple) and ImageJ software, respectively. PKC phosphorylation (in percentage) was determined by measuring the proportion of phosphorylated PKC (slower mobility band) over total PKC by densitometry.

SUPPLEMENTARY MATERIALS

stke.sciencemag.org/cgi/content/full/14/678/eabe4509/DC1

View/request a protocol for this paper from Bio-protocol.

REFERENCES AND NOTES

1. B. Nolen, S. Taylor, G. Ghosh, Regulation of protein kinases: Controlling activity through activation segment conformation. Mol. Cell 15, 661–675 (2004).

2. L. R. Pearce, D. Komander, D. R. Alessi, The nuts and bolts of A GC protein kinases. *Nat. Rev. Mol. cell Biol.* **11**, 9–22 (2010).

3. A. E. Leroux, J. O. Schulze, R. M. Biondi, AGC kinases, mechanisms of regulation and innovative drug development. *Semin. Cancer Biol.* **48**, 1–17 (2018).

4. A. Mora, D. Komander, D. M. F. Van Aalten, D. R. Alessi, PDK1, the master regulator of AGC kinase signal transduction. *Semin. Cell Dev. Biol.* **15**, 161–170 (2004).

5. D. R. Alessi, S. R. James, C. P. Downes, A. B. Holmes, P. R. J. Gaffney, C. B. Reese, P. Cohen, Characterization of a 3-phosphoinositide-dependent protein kinase which phosphorylates and activates protein kinase Bα. *Curr. Biol.* **7**, 261–269 (1997).

6. E. M. Dutil, A. Toker, A. C. Newton, Regulation of conventional protein kinase C isozymes by phosphoinositide-dependent kinase 1 (PDK-1). *Curr. Biol.* **8**, 1366–1375 (1998).

7. L. M. Keranen, E. M. Dutil, A. C. Newton, Protein kinase C is regulated in vivo by three functionally distinct phosphorylations. *Curr. Biol.* **5**, 1394–1403 (1995).

8. R. B. Pearson, P. B. Dennis, J. W. Han, N. A. Williamson, S. C. Kozma, R. E. Wettenhall, G. Thomas, The principal target of rapamycin-induced p70s6k inactivation is a novel phosphorylation site within a conserved hydrophobic domain. *EMBO J.* **14**, 5279–5287 (1995).

9. D. R. Alessi, M. Andjelkovic, B. Caudwell, P. Cron, N. Morrice, P. Cohen, B. A. Hemmings, Mechanism of activation of protein kinase B by insulin and IGF-1. *EMBO J.* **15**, 6541–6551 (1996).

10. A. S. Edwards, A. C. Newton, Phosphorylation at conserved carboxyl-terminal hydrophobic motif regulates the catalytic and regulatory domains of protein kinase C. *J. Biol. Chem.* **272**, 18382–18390 (1997).

11. G. Y. Liu, D. M. Sabatini, mTOR at the nexus of nutrition, growth, ageing and disease. *Nat. Rev. Mol. Cell Biol.* **21**, 183–203 (2020).

12. J. A. Le Good, W. H. Ziegler, D. B. Parekh, D. R. Alessi, P. Cohen, P. J. Parker, Protein kinase C isotypes controlled by phosphoinositide 3-kinase through the protein kinase PDK1. *Science* **281**, 2042–2045 (1998).

13. T. Ikenoue, K. Inoki, Q. Yang, X. Zhou, K.-L. Guan, Essential function of TORC2 in PKC and Akt turn motif phosphorylation, maturation and signalling. *EMBO J.* **27**, 1919–1931 (2008).

14. V. Facchinetti, W. Ouyang, H. Wei, N. Soto, A. Lazorchak, C. Gould, C. Lowry, A. C. Newton, Y. Mao, R. Q. Miao, W. C. Sessa, J. Qin, P. Zhang, B. Su, E. Jacinto, The mammalian target of rapamycin complex 2 controls folding and stability of Akt and protein kinase C. *EMBO J.* **27**, 1932–1943 (2008).

15. J. W. Orr, A. C. Newton, Requirement for negative charge on "activation loop" of protein kinase C. *J. Biol. Chem.* **269**, 27715–27718 (1994).

16. F. Bornancin, P. J. Parker, Phosphorylation of threonine 638 critically controls the dephosphorylation and inactivation of protein kinase Cα. *Curr. Biol.* **6**, 1114–1123 (1996).

17. W. J. Oh, C.-c. Wu, S. J. Kim, V. Facchinetti, L.-A. Julien, M. Finlan, P. P. Roux, B. Su, E. Jacinto, mTORC2 can associate with ribosomes to promote cotranslational phosphorylation and stability of nascent Akt polypeptide. *EMBO J.* **29**, 3939–3951 (2010).

18. T. O. Chan, S. E. Rittenhouse, P. N. Tsichlis, AKT/PKB and other D3 phosphoinositide-regulated kinases: Kinase activation by phosphoinositide-dependent phosphorylation. *Annu. Rev. Biochem.* **68**, 965–1014 (1999).

19. M. Ebner, I. Lučić, T. A. Leonard, I. Yudushkin, PI(3,4,5)P₃ engagement restricts Akt activity to cellular membranes. *Mol. Cell* **65**, 416–431.e6 (2017).

20. A. Klippel, W. M. Kavanaugh, D. Pot, L. T. Williams, A specific product of phosphatidylinositol 3-kinase directly activates the protein kinase Akt through its pleckstrin homology domain. *Mol. Cell. Biol.* **17**, 338–344 (1997).

21. M. Frech, M. Andjelkovic, E. Ingley, K. K. Reddy, J. R. Falck, B. A. Hemmings, High affinity binding of inositol phosphates and phosphoinositides to the pleckstrin homology domain of RAC/protein kinase B and their influence on kinase activity. *J. Biol. Chem.* **272**, 8474–8481 (1997).

22. T. F. Franke, D. R. Kaplan, L. C. Cantley, A. Toker, Direct regulation of the *Akt* proto-oncogene product by phosphatidylinositol-3,4-bisphosphate. *Science* **275**, 665–668 (1997).

23. N. Chu, A. L. Salguero, A. Z. Liu, Z. Chen, D. R. Dempsey, S. B. Ficarro, W. M. Alexander, J. A. Marto, Y. Li, L. M. Amzel, S. B. Gabelli, P. A. Cole, Akt kinase activation mechanisms revealed using protein semisynthesis. *Cell* **174**, 897–907.e14 (2018).

24. J. Yang, P. Cron, V. Thompson, V. M. Good, D. Hess, B. A. Hemmings, D. Barford, Molecular mechanism for the regulation of protein kinase B/Akt by hydrophobic motif phosphorylation. *Mol. Cell* **9**, 1227–1240 (2002).

25. N. Balasuriya, M. T. Kunkel, X. Liu, K. K. Biggar, S. S. C. Li, A. C. Newton, P. O'Donoghue, Genetic code expansion and live cell imaging reveal that Thr-308 phosphorylation is irreplaceable and sufficient for Akt1 activity. *J. Biol. Chem.* **293**, 10744–10756 (2018).

26. T. R. Baffi, K. Cohen-Katsenelson, A. C. Newton, PHLPPing the script: Emerging roles of PHLPP phosphatases in cell signaling. *Annu. Rev. Pharmacol. Toxicol.* **61**, 723–743 (2021).

27. D. D. Sarbassov, D. A. Guertin, S. M. Ali, D. M. Sabatini, Phosphorylation and regulation of Akt/PKB by the rictor-mTOR complex. *Science* **307**, 1098–1101 (2005).

28. D. R. Alessi, L. R. Pearce, J. M. García-Martínez, New insights into mTOR signaling: mTORC2 and beyond. *Sci. Signal.* **2**, pe27 (2009).

29. B. Su, E. Jacinto, Mammalian TOR signaling to the AGC kinases. *Crit. Rev. Biochem. Mol. Biol.* **46**, 527–547 (2011).

30. A. Toker, A. C. Newton, Akt/protein kinase B is regulated by autophosphorylation at the hypothetical PDK-2 site. *J. Biol. Chem.* **275**, 8271–8274 (2000).

31. A. Behn-Krappa, A. C. Newton, The hydrophobic phosphorylation motif of conventional protein kinase C is regulated by autophosphorylation. *Curr. Biol.* **9**, 728–737 (1999).

32. A. Balendran, A. Casamayor, M. Deak, A. Paterson, P. Gaffney, R. Currie, C. P. Downes, D. R. Alessi, PDK1 acquires PDK2 activity in the presence of a synthetic peptide derived from the carboxyl terminus of PRK2. *Curr. Biol.* **9**, 393–404 (1999).

33. N. A. Warfel, M. Niederst, A. C. Newton, Disruption of the interface between the pleckstrin homology (PH) and kinase domains of Akt protein is sufficient for hydrophobic motif site phosphorylation in the absence of mTORC2. *J. Biol. Chem.* **286**, 39122–39129 (2011).

34. J. M. Garcia-Martinez, D. R. Alessi, mTOR complex 2 (mTORC2) controls hydrophobic motif phosphorylation and activation of serum- and glucocorticoid-induced protein kinase 1 (SGK1). *Biochem. J.* **416**, 375–385 (2008).

35. C.-S. Yang, T. A. Melhuish, A. Spencer, L. Ni, Y. Hao, K. Jividen, T. E. Harris, C. Snow, H. F. Frierson Jr., D. Wotton, B. M. Paschal, The protein kinase C super-family member PKN is regulated by mTOR and influences differentiation during prostate cancer progression. *Prostate* **77**, 1452–1467 (2017).

36. Y. Kamada, Y. Fujioka, N. N. Suzuki, F. Inagaki, S. Wullschleger, R. Loewith, M. N. Hall, Y. Ohsumi, Tor2 directly phosphorylates the AGC kinase Ypk2 to regulate actin polarization. *Mol. Cell. Biol.* **25**, 7239–7248 (2005).

37. P.-C. Chou, S. Rajput, X. Zhao, C. Patel, D. Albaciete, W. J. Oh, H. Q. Daguplo, N. Patel, B. Su, G. Werlen, E. Jacinto, mTORC2 is involved in the induction of RSK phosphorylation by serum or nutrient starvation. *Cell* **9**, 1567 (2020).

38. F. M. Roelants, K. L. Leskoske, M. N. Martinez Marshall, M. N. Locke, J. Thorner, The TORC2-dependent signaling network in the yeast *Saccharomyces cerevisiae*. *Biomolecules* **7**, 66 (2017).

39. S. Isotani, K. Hara, C. Tokunaga, H. Inoue, J. Avruch, K. Yonezawa, Immunopurified mammalian target of rapamycin phosphorylates and activates p70 S6 kinase α in vitro. *J. Biol. Chem.* **274**, 34493–34498 (1999).

40. D. A. Guertin, D. M. Stevens, C. C. Thoreen, A. A. Burds, N. Y. Kalaany, J. Moffat, M. Brown, K. J. Fitzgerald, D. M. Sabatini, Ablation in mice of the mTORC components raptor, rictor, or mLST8 reveals that mTORC2 is required for signaling to Akt-FOXO and PKCα, but not S6K1. *Dev. Cell* **11**, 859–871 (2006).

41. P. E. Burnett, R. K. Barrow, N. A. Cohen, S. H. Snyder, D. M. Sabatini, RAFT1 phosphorylation of the translational regulators p70 S6 kinase and 4E-BP1. *Proc. Natl. Acad. Sci.* **95**, 1432–1437 (1998).

42. D. D. Sarbassov, S. M. Ali, D.-H. Kim, D. A. Guertin, R. R. Latek, H. Erdjument-Bromage, P. Tempst, D. M. Sabatini, Rictor, a novel binding partner of mTOR, defines a rapamycin-insensitive and raptor-independent pathway that regulates the cytoskeleton. *Curr. Biol.* **14**, 1296–1302 (2004).

43. E. Jacinto, V. Facchinetti, D. Liu, N. Soto, S. Wei, S. Y. Jung, Q. Huang, J. Qin, B. Su, SIN1/MIP1 maintains rictor-mTOR complex integrity and regulates Akt phosphorylation and substrate specificity. *Cell* **127**, 125–137 (2006).

44. Q. Yang, K. Inoki, T. Ikenoue, K. L. Guan, Identification of Sin1 as an essential TORC2 component required for complex formation and kinase activity. *Genes Dev.* **20**, 2820–2832 (2006).

45. M. A. Frias, C. C. Thoreen, J. D. Jaffe, W. Schroder, T. Sculley, S. A. Carr, D. M. Sabatini, mSin1 is necessary for Akt/PKB phosphorylation, and its isoforms define three distinct mTORC2s. *Curr. Biol.* **16**, 1865–1870 (2006).

46. T. R. Baffi, A.-A. N. Van, W. Zhao, G. B. Mills, A. C. Newton, Protein kinase C quality control by phosphatase PHLPP1 unveils loss-of-function mechanism in cancer. *Mol. Cell* **74**, 378–392.e5 (2019).

47. J. D. Violin, J. Zhang, R. Y. Tsien, A. C. Newton, A genetically encoded fluorescent reporter reveals oscillatory phosphorylation by protein kinase C. *J. Cell Biol.* **161**, 899–909 (2003).

48. B. L. Ross, B. Tenner, M. L. Markwardt, A. Zviman, G. Shi, J. P. Kerr, N. E. Snell, J. J. McFarland, J. R. Mauban, C. W. Ward, M. A. Rizzo, J. Zhang, Single-color, ratiometric biosensors for detecting signaling activities in live cells. *eLife* **7**, e35458 (2018).

49. C. C. Thoreen, S. A. Kang, J. W. Chang, Q. Liu, J. Zhang, Y. Gao, L. J. Reichling, T. Sim, D. M. Sabatini, N. S. Gray, An ATP-competitive mammalian target of rapamycin inhibitor reveals rapamycin-resistant functions of mTORC1. *J. Biol. Chem.* **284**, 8023–8032 (2009).

50. C. M. Gould, C. E. Antal, G. Reyes, M. T. Kunkel, R. A. Adams, A. Ziyar, T. Riveros, A. C. Newton, Active site inhibitors protect protein kinase C from dephosphorylation and stabilize its mature form. *J. Biol. Chem.* **286**, 28922–28930 (2011).

51. C. E. Antal, J. D. Violin, M. T. Kunkel, S. Skovso, A. C. Newton, Intramolecular conformational changes optimize protein kinase C signaling. *Chem. Biol.* **21**, 459–469 (2014).

52. G. H. Iyer, M. J. Moore, S. S. Taylor, Consequences of lysine 72 mutation on the phosphorylation and activation state of cAMP-dependent kinase. *J. Biol. Chem.* **280**, 8800–8807 (2005).

53. D. R. Dries, L. L. Gallegos, A. C. Newton, A single residue in the C1 domain sensitizes novel protein kinase C isoforms to cellular diacylglycerol production. *J. Biol. Chem.* **282**, 826–830 (2007).

54. E. M. Dutil, A. C. Newton, Dual role of pseudosubstrate in the coordinated regulation of protein kinase C by phosphorylation and diacylglycerol. *J. Biol. Chem.* **275**, 10697–10701 (2000).

55. D. D. Sarbassov, S. M. Ali, D. M. Sabatini, Growing roles for the mTOR pathway. *Curr. Opin. Cell Biol.* **17**, 596–603 (2005).

56. L. Yan, V. Mieulet, R. F. Lamb, mTORC2 is the hydrophobic motif kinase for SGK1. *Biochem. J.* **416**, e19–e21 (2008).

57. N. Kannan, N. Haste, S. S. Taylor, A. F. Neuwald, The hallmark of AGC kinase functional divergence is its C-terminal tail, a cis-acting regulatory module. *Proc. Natl. Acad. Sci. U.S.A.* **104**, 1272–1277 (2007).

58. N. Grodsky, Y. Li, D. Bouzida, R. Love, J. Jensen, B. Nodes, J. Nonomiya, S. Grant, Structure of the catalytic domain of human protein kinase C β II complexed with a bisindolylmaleimide inhibitor. *Biochemistry* **45**, 13970–13981 (2006).

59. H. Tatebe, S. Murayama, T. Yonekura, T. Hatano, D. Richter, T. Furuya, S. Kataoka, K. Furuita, C. Kojima, K. Shiozaki, Substrate specificity of TOR complex 2 is determined by a ubiquitin-fold domain of the Sin1 subunit. *eLife* **6**, e19594 (2017).

60. A. J. M. Cameron, M. D. Linch, A. T. Saurin, C. Escribano, P. J. Parker, mTORC2 targets AGC kinases through Sin1-dependent recruitment. *Biochem. J.* **439**, 287–297 (2011).

61. J. D. Sweatt, C. M. Atkins, J. Johnson, J. D. English, E. D. Roberson, S.-J. Chen, A. Newton, E. Klann, Protected-site phosphorylation of protein kinase C in hippocampal long-term potentiation. *J. Neurochem.* **71**, 1075–1085 (2002).

62. P. V. Hornbeck, B. Zhang, B. Murray, J. M. Kornhauser, V. Latham, E. Skrzypek, PhosphoSitePlus, 2014: Mutations, PTMs and recalibrations. *Nucleic Acids Res.* **43**, D512–D520 (2015).

63. H. Tatebe, K. Shiozaki, Evolutionary conservation of the components in the TOR signaling pathways. *Biomolecules* **7**, 77 (2017).

64. M. T. Kunkel, Q. Ni, R. Y. Tsien, J. Zhang, A. C. Newton, Spatio-temporal dynamics of protein kinase B/Akt signaling revealed by a genetically encoded fluorescent reporter. *J. Biol. Chem.* **280**, 5581–5587 (2005).

65. R. A. Romano, N. Kannan, A. P. Kornev, C. J. Allison, S. S. Taylor, A chimeric mechanism for polyvalent trans-phosphorylation of PKA by PDK1. *Protein Sci.* **18**, 1486–1497 (2009).

66. M. Frödin, T. L. Antal, B. A. Dümmler, C. J. Jensen, M. Deak, S. Gammeltoft, R. M. Biondi, A phosphoserine/threonine-binding pocket in AGC kinases and PDK1 mediates activation by hydrophobic motif phosphorylation. *EMBO J.* **21**, 5396–5407 (2002).

67. R. M. Biondi, P. C. F. Cheung, A. Casamayor, M. Deak, R. A. Currie, D. R. Alessi, Identification of a pocket in the PDK1 kinase domain that interacts with PIF and the C–terminal residues of PKA. *EMBO J.* **19**, 979–988 (2000).

68. T. Gao, A. Toker, A. C. Newton, The carboxyl terminus of protein kinase C provides a switch to regulate its interaction with the phosphoinositide-dependent kinase, PDK-1. *J. Biol. Chem.* **276**, 19588–19596 (2001).

69. F. Enzler, P. Tschaikner, R. Schneider, E. Stefan, KinCon: Cell-based recording of full-length kinase conformations. *IUBMB Life* **72**, 1168–1174 (2020).

70. R. Röck, J. E. Mayrhofer, O. Torres-Quesada, F. Enzler, A. Raffeiner, P. Raffeiner, A. Feichtner, R. G. Huber, S. Koide, S. S. Taylor, J. Troppmair, E. Stefan, BRAF inhibitors promote intermediate BRAF(V600E) conformations and binary interactions with activated RAS. *Sci. Adv.* **5**, eaav8463 (2019).

71. E. Stefan, S. Aquin, N. Berger, C. R. Landry, B. Nyfeler, M. Bouvier, S. W. Michnick, Quantification of dynamic protein complexes using Renilla luciferase fragment complementation applied to protein kinase A activities in vivo. *Proc. Natl. Acad. Sci. U.S.A.* **104**, 16916–16921 (2007).

72. R. Röck, V. Bachmann, H.-e. C. Bhang, M. Malleshaiah, P. Raffeiner, J. E. Mayrhofer, P. M. Tschaikner, K. Bister, P. Aanstad, M. G. Pomper, S. W. Michnick, E. Stefan, In-vivo detection of binary PKA network interactions upon activation of endogenous GPCRs. *Sci. Rep.* **5**, 11133 (2015).

73. C. E. Schafmeister, J. Po, G. L. Verdine, An all-hydrocarbon cross-linking system for enhancing the helicity and metabolic stability of peptides. *J. Am. Chem. Soc.* **122**, 5891–5892 (2000).

74. G. L. Verdine, G. J. Hilinski, in *Methods in Enzymology* (Academic Press Inc., 2012), vol. 503, pp. 3–33.

75. M. A. Lemmon, J. Schlessinger, Cell signaling by receptor tyrosine kinases. *Cell* **141**, 1117–1134 (2010).

76. A. J. Flint, R. D. Paladini, D. E. Koshland Jr., Autophosphorylation of protein kinase C at three separated regions of its primary sequence. *Science* **249**, 408–411 (1990).

77. M. M. Keshwani, C. Klammt, S. von Daake, Y. Ma, A. P. Kornev, S. Choe, P. A. Insel, S. S. Taylor, Cotranslational cis-phosphorylation of the COOH-terminal tail is a key

78. priming step in the maturation of cAMP-dependent protein kinase. *Proc. Natl. Acad. Sci. U.S.A.* **109**, E1221–E1229 (2012).

78. C. Hauge, T. L. Antal, D. Hirschberg, U. Doehn, K. Thorup, L. Idrissova, K. Hansen, O. N. Jensen, T. J. Jorgensen, R. M. Biondi, M. Frodin, Mechanism for activation of the growth factor-activated AGC kinases by turn motif phosphorylation. *EMBO J.* **26**, 2251–2261 (2007).

79. A. Toker, A. C. Newton, Cellular signaling: Pivoting around PDK-1. *Cell* **103**, 185–188 (2000).

80. M. Y. Hein, N. C. Hubner, I. Poser, J. Cox, N. Nagaraj, Y. Toyoda, I. A. Gak, I. Weisswange, J. Mansfeld, F. Buchholz, A. A. Hyman, M. Mann, A human interactome in three quantitative dimensions organized by stoichiometries and abundances. *Cell* **163**, 712–723 (2015).

81. S. M. Ali, D. M. Sabatini, Structure of S6 kinase 1 determines whether raptor-mTOR or rictor-mTOR phosphorylates its hydrophobic motif site. *J. Biol. Chem.* **280**, 19445–19448 (2005).

82. S. S. Schalm, J. Blenis, Identification of a conserved motif required for mTOR signaling. *Curr. Biol.* **12**, 632–639 (2002).

83. A. Romanelli, V. C. Dreisbach, J. Blenis, Characterization of phosphatidylinositol 3-kinase-dependent phosphorylation of the hydrophobic motif site Thr389 in p70 S6 kinase 1. *J. Biol. Chem.* **277**, 40281–40289 (2002).

84. N. Pullen, P. B. Dennis, M. Andjelkovic, A. Dufner, S. C. Kozma, B. A. Hemmings, G. Thomas, Phosphorylation and activation of p70^{s6k} by PDK1. *Science* **279**, 707–710 (1998).

85. D. M. Sabatini, Twenty-five years of mTOR: Uncovering the link from nutrients to growth. *Proc. Natl. Acad. Sci. U.S.A.* **114**, 11818–11825 (2017).

86. C. Hauge, M. Frödin, RSK and MSK in MAP kinase signalling. *J. Cell Sci.* **119**, 3021–3023 (2006).

87. J. Beenstock, N. Mooshayef, D. Engelberg, How do protein kinases take a selfie (autophosphorylate)? *Trends Biochem. Sci.* **41**, 938–953 (2016).

88. A. C. Newton, D. E. Koshland Jr., Protein kinase C autophosphorylates by an intrapeptide reaction. *J. Biol. Chem.* **262**, 10185–10188 (1987).

89. E. M. Dutil, L. M. Keranen, A. A. DePaoli-Roach, A. C. Newton, In vivo regulation of protein kinase C by trans-phosphorylation followed by autophosphorylation. *J. Biol. Chem.* **269**, 29359–29362 (1994).

90. A. J. M. Cameron, C. Escribano, A. T. Saurin, B. Kostelecky, P. J. Parker, PKC maturation is promoted by nucleotide pocket occupation independently of intrinsic kinase activity. *Nat. Struct. Mol. Biol.* **16**, 624–630 (2009).

91. P. A. Cole, N. Chu, A. L. Salguero, H. Bae, AKTivation mechanisms. *Curr. Opin. Struct. Biol.* **59**, 47–53 (2019).

92. C. J. Swanson, M. Ritt, W. Wang, M. J. Lang, A. Narayan, J. J. Tesmer, M. Westfall, S. Sivaramakrishnan, Conserved modular domains team up to latch-open active protein kinase Cα. *J. Biol. Chem.* **289**, 17812–17829 (2014).

93. S.-M. Huang, P. S. Leventhal, G. J. Wiepz, P. J. Bertics, Calcium and phosphatidylserine stimulate the self-association of conventional protein kinase C Isoforms. *Biochemistry* **38**, 12020–12027 (1999).

94. B. P. Ziemba, J. Li, K. E. Landgraf, J. D. Knight, G. A. Voth, J. J. Falke, Single-molecule studies reveal a hidden key step in the activation mechanism of membrane-bound protein kinase C-α. *Biochemistry* **53**, 1697–1713 (2014).

95. Y. A. Hannun, R. M. Bell, Phorbol ester binding and activation of protein kinase C on triton X-100 mixed micelles containing phosphatidylserine. *J. Biol. Chem.* **261**, 9341–9347 (1986).

96. X. Hui, B. Sauer, L. Kaestner, K. Kruse, P. Lipp, PKCα diffusion and translocation are independent of an intact cytoskeleton. *Sci. Rep.* **7**, 475 (2017).

97. C. E. Antal, J. A. Callender, A. P. Kornev, S. S. Taylor, A. C. Newton, Intramolecular C2 domain-mediated autoinhibition of protein kinase βII. *Cell Rep.* **12**, 1252–1260 (2015).

98. H. Dudek, S. R. Datta, T. F. Franke, M. J. Birnbaum, R. Yao, G. M. Cooper, R. A. Segal, D. R. Kaplan, M. E. Greenberg, Regulation of neuronal survival by the serine-threonine protein kinase Akt. *Science* **275**, 661–665 (1997).

99. K. Datta, T. F. Franke, T. O. Chan, A. Makris, S. I. Yang, D. R. Kaplan, D. K. Morrison, E. A. Golemis, P. N. Tsichlis, AH/PH domain-mediated interaction between Akt molecules and its potential role in Akt regulation. *Mol. Cell. Biol.* **15**, 2304–2310 (1995).

100. L.-C. Huang, K. E. Ross, T. R. Baffi, H. Drabkin, K. J. Kochut, Z. Ruan, P. D'Eustachio, D. McSkimming, C. Arighi, C. Chen, D. A. Natale, C. Smith, P. Gaudet, A. C. Newton, C. Wu, N. Kannan, Integrative annotation and knowledge discovery of kinase post-translational modifications and cancer-associated mutations through federated protein ontologies and resources. *Sci. Rep.* **8**, 6518 (2018).

101. C. E. Antal, A. M. Hudson, E. Kang, C. Zanca, C. Wirth, N. L. Stephenson, E. W. Trotter, L. L. Gallegos, C. J. Miller, F. B. Furnari, T. Hunter, J. Brognard, A. C. Newton, Cancer-associated protein kinase C mutations reveal kinase's role as tumor suppressor. *Cell* **160**, 489–502 (2015).

102. A. C. Newton, J. Brognard, Reversing the paradigm: Protein kinase C as a tumor suppressor. *Trends Pharmacol. Sci.* **38**, 438–447 (2017).

103. T. L. Yuan, L. C. Cantley, PI3K pathway alterations in cancer: Variations on a theme. *Oncogene* **27**, 5497–5510 (2008).

104. T. Tian, X. Li, J. Zhang, mTOR signaling in cancer and mTOR inhibitors in solid tumor targeting therapy. *Int. J. Mol. Sci.* **20**, 755 (2019).

105. V. S. Rodrik-Outmezguine, M. Okaniwa, Z. Yao, C. J. Novotny, C. McWhirter, A. Banaji, H. Won, W. Wong, M. Berger, E. De Stanchina, D. G. Barratt, S. Cosulich, T. Klinowska, N. Rosen, K. M. Shokat, Overcoming mTOR resistance mutations with a new-generation mTOR inhibitor. *Nature* **534**, 272–276 (2016).

106. C. C. Uphoff, H. G. Drexler, in *Cancer Cell Culture: Methods and Protocols*, I. A. Cree, Ed. (Humana Press, 2011), pp. 93–103; https://doi.org/10.1007/978-1-61779-080-5_8.

107. S. F. Altschul, W. Gish, W. Miller, E. W. Myers, D. J. Lipman, Basic local alignment search tool. *J. Mol. Biol.* **215**, 403–410 (1990).

108. K. Katoh, MAFFT: A novel method for rapid multiple sequence alignment based on fast Fourier transform. *Nucleic Acids Res.* **30**, 3059–3066 (2002).

109. A. F. Neuwald, Rapid detection, classification and accurate alignment of up to a million or more related protein sequences. *Bioinformatics* **25**, 1869–1875 (2009).

110. G. Manning, D. B. Whyte, R. Martinez, T. Hunter, S. Sudarsanam, The protein kinase complement of the human genome. *Science* **298**, 1912–1934 (2002).

111. G. E. Crooks, G. Hon, J.-M. Chandonia, S. E. Brenner, WebLogo: A sequence logo generator. *Genome Res.* **14**, 1188–1190 (2004).

112. L. L. Gallegos, M. T. Kunkel, A. C. Newton, Targeting protein kinase C activity reporter to discrete intracellular regions reveals spatiotemporal differences in agonist-dependent signaling. *J. Biol. Chem.* **281**, 30947–30956 (2006).

113. G. Martiny-Baron, M. G. Kazanietz, H. Mischak, P. M. Blumberg, G. Kochs, H. Hug, D. Marme, C. Schachtele, Selective inhibition of protein kinase C isozymes by the indolocarbazole Gö 6976. *J. Biol. Chem.* **268**, 9194–9197 (1993).

114. M. Gschwendt, S. Dieterich, J. Rennecke, W. Kittstein, H. J. Mueller, F. J. Johannes, Inhibition of protein kinase C μ by various inhibitors. Differentiation from protein kinase c isoenzymes. *FEBS Lett.* **392**, 77–80 (1996).

115. J. Lin, D. Sampath, M. A. Nannini, B. B. Lee, M. Degtyarev, J. Oeh, H. Savage, Z. Guan, R. Hong, R. Kassees, L. B. Lee, T. Risom, S. Gross, B. M. Liederer, H. Koeppen, N. J. Skelton, J. J. Wallin, M. Belvin, E. Punnoose, L. S. Friedman, K. Lin, Targeting activated Akt with GDC-0068, a novel selective Akt inhibitor that is efficacious in multiple tumor models. *Clin. Cancer Res.* **19**, 1760–1772 (2013).

116. L. R. Pearce, E. M. Sommer, K. Sakamoto, S. Wullschleger, D. R. Alessi, Protor-1 is required for efficient mTORC2-mediated activation of SGK1 in the kidney. *Biochem. J.* **436**, 169–179 (2011).

117. J. D. Lapek Jr., M. K. Lewinski, J. M. Wozniak, J. Guatelli, D. J. Gonzalez, Quantitative temporal viromics of an inducible HIV-1 model yields insight to global host targets and phospho-dynamics associated with protein Vpr. *Mol. Cell. Proteomics* **16**, 1447–1461 (2017).

118. National Research Council (US) Committee for the Update of the Guide for the Care and Use of Laboratory Animals, *Guide for the Care and Use of Laboratory Animals* (National Academies Press, 2011).

119. D. Kozakov, D. R. Hall, B. Xia, K. A. Porter, D. Padhorny, C. Yueh, D. Beglov, S. Vajda, The ClusPro web server for protein-protein docking. *Nat. Protoc.* **12**, 255–278 (2017).

120. Schrodinger LLC, The PyMOL Molecular Graphics System, Version 1.8 (2015).

121. K. S. Metz, E. M. Deoudes, M. E. Berginski, I. Jimenez-Ruiz, B. A. Aksoy, J. Hammerbacher, S. M. Gomez, D. H. Phanstiel, Coral: Clear and customizable visualization of human kinome data. *Cell Syst.* **7**, 347–350.e1 (2018).

122. C. M. Gould, N. Kannan, S. S. Taylor, A. C. Newton, The chaperones Hsp90 and Cdc37 mediate the maturation and stabilization of protein kinase C through a conserved PXXP motif in the C-terminal tail. *J. Biol. Chem.* **284**, 4921–4935 (2009).

123. D. I. McSkimming, S. Dastgheib, T. R. Baffi, D. P. Byrne, S. Ferries, S. T. Scott, A. C. Newton, C. E. Eyers, K. J. Kochut, P. A. Eyers, N. Kannan, KinView: A visual comparative sequence analysis tool for integrated kinome research. *Mol. Biosyst.* **12**, 3651–3665 (2016).

124. Z.-B. Xu, D. Chaudhary, S. Olland, S. Wolfrom, R. Czerwinski, K. Malakian, L. Lin, M. L. Stahl, D. Joseph-McCarthy, C. Benander, L. Fitz, R. Greco, W. S. Somers, L. Mosyak, Catalytic domain crystal structure of protein kinase C-θ (PKCθ). *J. Biol. Chem.* **279**, 50401–50409 (2004).

125. M. J. van Eis, J.-P. Evenou, P. Floersheim, C. Gaul, S. W. Cowan-Jacob, L. Monovich, G. Rummel, W. Schuler, W. Stark, A. Strauss, A. von Matt, E. Vangrevelinghe, J. Wagner, N. Soldermann, 2,6-Naphthyridines as potent and selective inhibitors of the novel protein kinase C isozymes. *Bioorg. Med. Chem. Lett.* **21**, 7367–7372 (2011).

126. K. Lin, J. Lin, W.-I. Wu, J. Ballard, B. B. Lee, S. L. Gloor, G. P. A. Vigers, T. H. Morales, L. S. Friedman, N. Skelton, B. J. Brandhuber, An ATP-site on-off switch that restricts phosphatase accessibility of Akt. *Sci. Signal.* **5**, ra37 (2012).

127. D. R. Knighton, J. H. Zheng, L. F. Ten Eyck, V. A. Ashford, N. H. Xuong, S. S. Taylor, J. M. Sowadski, Crystal structure of the catalytic subunit of cyclic adenosine monophosphate-dependent protein kinase. *Science* **253**, 407–414 (1991).

128. T. A. Leonard, B. Różycki, L. F. Saidi, G. Hummer, J. H. Hurley, Crystal structure and allosteric activation of protein kinase βII. *Cell* **144**, 55–66 (2011).

129. T. Katoh, T. Takai, T. Yukawa, T. Tsukamoto, E. Watanabe, H. Mototani, T. Arita, H. Hayashi, H. Nakagawa, M. G. Klein, H. Zou, B. C. Sang, G. Snell, Y. Nakada, Discovery and optimization of 1,7-disubstituted-2,2-dimethyl-2,3-dihydroquinazolin-4(1H)-ones as potent and selective PKCθ inhibitors. *Bioorg. Med. Chem.* **24**, 2466–2475 (2016).

130. C. S. Gibbs, M. J. Zoller, Rational scanning mutagenesis of a protein kinase identifies functional regions involved in catalysis and substrate interactions. *J. Biol. Chem.* **266**, 8923–8931 (1991).

Science Signaling

mTORC2 controls the activity of PKC and Akt by phosphorylating a conserved TOR interaction motif

Timothy R. Baffi, Gema Lordén, Jacob M. Wozniak, Andreas Feichtner, Wayland Yeung, Alexandr P. Kornev, Charles C. King, Jason C. Del Rio, Ameya J. Limaye, Julius Bogomolovas, Christine M. Gould, Ju Chen, Eileen J. Kennedy, Natarajan Kannan, David J. Gonzalez, Eduard Stefan, Susan S. Taylor and Alexandra C. Newton

mTORC2 marks kinases for maturity

The activity of members of the AGC family of kinases, which includes Akt and PKC, requires multiple phosphorylation events at different sites. As part of the mTORC2 complex, the kinase mTOR has been proposed to catalyze the phosphorylation of one of these sites termed the hydrophobic motif. Baffi *et al.* identified a distinct and evolutionarily conserved motif in Akt and PKC termed the TOR interaction motif (TIM) whose phosphorylation by mTORC2 was required for catalytic competence. Newly synthesized PKC dimerized through the TIM, and phosphorylation of the TIM in PKC by mTORC2 abolished this dimerization, ultimately leading to autophosphorylation of the hydrophobic motif. These results resolve long-standing conflicts about the role of mTORC2 in AGC kinase maturation and highlight a potential negative effect of mTOR kinase inhibitors that are now in clinical development.

ARTICLE TOOLS	http://stke.sciencemag.org/content/14/678/eabe4509
SUPPLEMENTARY MATERIALS	http://stke.sciencemag.org/content/suppl/2021/04/09/14.678.eabe4509.DC1
RELATED CONTENT	http://stke.sciencemag.org/content/sigtrans/13/657/eabc1328.full http://stke.sciencemag.org/content/sigtrans/12/585/eaav3249.full http://science.sciencemag.org/content/sci/370/6513/eabc2754.full http://science.sciencemag.org/content/sci/367/6480/912.full http://advances.sciencemag.org/content/advances/6/45/eabc1251.full
REFERENCES	This article cites 126 articles, 60 of which you can access for free http://stke.sciencemag.org/content/14/678/eabe4509#BIBL
PERMISSIONS	http://www.sciencemag.org/help/reprints-and-permissions

Use of this article is subject to the Terms of Service